A passive pHRI controller for assisting the user in partially known tasks

Dimitrios Papageorgiou[1,2], *Member, IEEE,* Theodora Kastritsi[2], *Student member, IEEE,* Zoe Doulgeri[1,2], *Senior member, IEEE,* George A. Rovithakis[1,2], *Senior member, IEEE,*

***Abstract*—In this work, a passive physical human-robot interaction (pHRI) controller is proposed to enhance pHRI performance in terms of precision, cognitive load and user effort, in cases partial knowledge of the task is available. Partial knowledge refers to a subspace of SE(3) determined by the desired task, generally mixing both position and orientation variables and which is mathematically approximated by parametric expressions. The proposed scheme, which utilizes the notion of virtual constraints and the prescribed performance control methodology, is proved to be passive with respect to the interaction force, while guaranteeing constraint satisfaction in all cases. The control scheme, is experimentally validated and compared with a dissipative control scheme utilizing a KUKA LWR4+ robot in a master-slave task; experiments also include an application to a robotic assembly case.**

***Index Terms*—physical human-robot interaction, active constraints, robot control, passivity**

I. Introduction

The development of light multi-degree of freedom (dof) human scale robots, with the ability to estimate or measure external forces, enables physical human-robot interaction (pHRI), thus opening new robot application avenues. For instance, human robot collaboration has already showed promising results in terms of efficiency and performance [1], [2]; the human contributes with his experience, knowledge and cognition, regarding the execution of the task, while the robot reduces the user effort and cognitive load needed to accomplish the task [3] and increases accuracy [4]. In the robotic task programming issue, kinesthetic teaching has been utilized to incrementally learn a task [5], reducing the duration needed for its programming. Moreover, as kinesthetic guidance provides an intuitive interface to the human-teacher, allowing the user to navigate the robot with his hands, he is no longer required to possess any skills in robot programming.

[1]D.Papageorgiou, Z. Doulgeri and G. A. Rovithakis are with the Center for Research and Technology Hellas (CERTH), Greece e-mails: dimpapag@iti.gr, doulgeri@iti.gr, robi@iti.gr

[2]Authors are with the Dept. of Electrical and Computer Engineering, Aristotle University of Thessaloniki, Greece e-mails: dimpapag@eng.auth.gr, tkastrit@ece.auth.gr, doulgeri@eng.auth.gr, robi@eng.auth.gr

Manuscript received [Month] [No], [Year]; revised [Month] [No], [Year].

The research leading to these results has received funding by the EU Horizon 2020 Research and Innovation Programme, under grant agreement No 644938, project Sarafun and partially under grant agreement No 820767, project CoLLaboratE.

Regarding Theodora Kastritsi:«This research is co-financed by Greece and the European Union (European Social Fund- ESF) through the Operational Programme «Human Resources Development, Education and Lifelong Learning»in the context of the project "Strengthening Human Resources Research Potential via Doctorate Research" (MIS-5000432), implemented by the State Scholarships Foundation (IKY)».

As pHRI copes with the actual exchange of forces and physical power between the human and the robot, the primary key issue that needs to be resolved by the robot's controller concerns safety and dependability. Safety, is often studied in terms of passive (inherent) and active compliance in the robot control literature. Passive compliance involves specialized hardware and is crucial in high frequency contacts like collisions with rigid environments, while active compliance can be useful in human robot interactions, which happen at a slower frequency range. The prominent motion control approach, which provides a robot with a compliant behavior, is impedance control introduced by Hogan [6]. Under impedance control, the robot acts as a mechanical impedance with desired parameters, or as a mechanical admittance [7]. Impedance control assumes knowledge of the robot's dynamic model and its environment as well as availability of interaction force measurements, to decouple the system [7].

Physical human-robot interaction can be discriminated between two categories, namely intentional and unintentional, as seen from the side of human user. Some works focus on the classification of contact between those categories based on interaction forces e.g., [8], and others on collision reaction strategies [9], [10] according to human safety standards [11].

In intentional pHRI tasks, an important key issue that needs to be addressed by the robot's controller concern the robot's quality-of-performance. In pHRI tasks, robot performance concerns the robot's ability to adapt its behavior dynamically according to the task and the human intentions. The reported works on pHRI performance can be distinguished in two categories, those for which the robot does not use any knowledge of the task and those for which the robot exploits partial knowledge of the task, which is assumed to be or made available.

When there is no knowledge about the task, impedance control with zero target stiffness is utilized, to allow the system to be fully compliant, as well as impedance parameter modulation to enhance the performance of the robot during the execution of the task under human guidance. An adaptive admittance/impedance control scheme, inspired by human studies, is proposed in [12], switching damping between two values according to the end-effector velocity. In [13], the damping value is calculated on-line to minimize a cost function related to both the value of damping and its rate. In [14], the derivative of the forces is used to adjust damping. In [15], a fuzzy learning method to calculate on-line the damping is proposed. Although all the above works adjust only the target damping parameter, in [16], the inertia parameter is also adjusted to maintain constant the bandwidth of the overall system. In this direction, some works propose the adjustment of both damping and inertial parameters, according to velocity [17] or acceleration estimates [16]. In other works, [18], [19], the parameters of the impedance model are adapted to maintain stability of the coupled human-robot system, based on the detection of undesired oscillations. Moreover, human intention prediction is used either to adapt the target admittance [20], or to reshape the nominal path [21], [22] during pHRI. In [23], an automatic smooth transition between interaction modes is proposed, to provide precision and comfort during pHRI in free space, and enable force amplification when the robot is in contact with its environment.

In many cognitive-demanding pHRI applications (e.g., robot assisted minimally invasive surgery, car assembly), partial knowledge of the task exists [24], [25]. By exploiting this knowledge, the cognitive load of the user could be reduced, resulting in higher accuracy, faster completion and less fatigue for the user. In the literature, there are many works that exploit partial knowledge of the task to enhance pHRI performance either in the form of a human intension model or in the form of virtual task constraints. In the cooperative lifting [26] or the planar manipulation of a heavy object [27] a high level knowledge of the task between humans is used. In particular, in [26] a human intention prediction scheme is proposed based on the minimum jerk model, while in [27] the human motion is modeled as a revolute joint and the parameters of the motion are estimated on-line based on force/torque measurements. In [28] an adaptive dynamical system with a stable limit cycle is utilized to model human hand-shaking. Task knowledge with respect to its spatial characteristics is exploited in [29] in terms of a predefined desired path, where an admittance controller for fast point-to-point cooperative sliding of an object is proposed, utilizing a Kalman filter to estimate the parameters of the minimum jerk velocity profile. In a cooperative manipulation task addressed in [30] the full knowledge of the task dynamics and kinematics as well as the desired trajectory is assumed to be available; the authors propose a role allocation policy to distribute the effort among the participants, according to interaction force measurements. Knowledge of the task's scene in the form of "virtual fixtures" (VF), also known as "active constraints" (AC), are considered in many works, particularly involving robotic surgery applications. Active constraints were firstly introduced in tele-robotic manipulation [3], [31] and have been utilized in surgical, industrial [32], [25], or even in underwater robotic tasks, [33] to enhance operator performance in terms of execution time, precision and error rates. VFs are placed based on prior partial knowledge of the task and/or environment and provide the user with haptic cues, relieving, in this way, some of his/her cognitive burden, similarly to the physical assistance given by a ruler while drawing a line [3]. The use of VF or AC has also been considered a special application of shared control [34]. Haptic shared control is shown to improve task performance, control effort and operator cognitive workload in telemanipulation tasks in [35]. A recent review of shared control in cooperative pHRI tasks is given in [36].

A more detailed review of the implementations of VFs in surgical tasks can be found in [37]. The works of [38], [39], consider a parametric analytic expression of a given reference path and propose anisotropic damping - in an admittance control law - to facilitate the user in a surgery task, discouraging motions close to the constraints. However, the orientation is not taken into consideration. In [40], a target stiffness is introduced in the 6D end-effector space in addition to damping, having as an equilibrium a desired path and a desired orientation that are not coupled. In [41] a dissipative control scheme is proposed, considering position-orientation couplings, for complete pose control, employing energy redirection for increased task accuracy. However, this approach does not guarantee constraint satisfaction in all cases. In [42] a control scheme for virtual fixture enforcement and adaptation is proposed, which involves parametric expressions of oriented paths and penetrable virtual fixtures.

In this work, we consider the case of a generic task, for which partial knowledge is available with respect to a 6D work subspace of the robot's end-effector, which may include both position and orientation variables. This subspace is mathematically modeled by parametric expressions, reflecting the desired task; parameters may couple position and orientation variables depending on the task. Utilizing the notion of virtual fixtures, we propose a robot control scheme that enhances pHRI performance in terms of precision, cognitive load and user effort by enforcing virtual constraints around the subspace of $SE(3)$ defined by the partial knowledge of the task. The closed loop system is proved to be passive with respect to the interaction force, while guaranteeing constraint satisfaction in all cases. Moreover, it is shown experimentally that in a 3D oriented path task, it achieves better performance as compared to the dissipative controller [41]. The proposed approach is illustrated experimentally in an robotic assembly task of a mobile phone. The proposed controller design draws on the Prescribed Performance Control (PPC) methodology, which was firstly introduced in [43] and extended to the approximation-free case in [44], [45], [46]. It has been applied in the design of robot position controllers [47], [48], [49], [50], in force/position control [51], in contact establishment [52], in constrained visual servoing in [53], as well as to impose constraints during the robot's autonomous operation [54], [55] [56], [57]. The contribution of the proposed scheme lies (a) in its generalized formulation which incorporates (i) partial task knowledge even in cases where position and orientation variables are coupled (ii) task uncertainty in the degree of parameterization and the maximum allowable deviations of the end-effector pose, thus greatly accelerating the pHRI task and (b) on the rigorous stability proof of the proposed virtual constraint controller, which includes not only the strictly output passivity of the interaction force with respect to the robot's end-effector velocity, but also the boundedness of all closed loop signals which implies the satisfaction of the virtual constraints at all times.

The rest of the paper is organized as follows. In Section II, the parametric modeling of partially known task is described and some representative examples are given. The problem description and the control objectives are explained in Section III. In Section IV, the calculation of the nearest to desired pose is detailed. In Section V, the control signal is developed and the proofs of passivity and state boundedness are given. An experimental evaluation of the proposed control scheme is developed in Section VI, followed by a discussion on its significance and limitation at Section VIIand, finally, conclusions are drawn in Section VIII. Preliminaries and certain proof details are provided in Appendices A and B.

II. Parametric Modeling of Partially known Tasks

Consider a N-dof robotic manipulator, whose joint variables are denoted by $\mathbf{q} \in \mathbb{R}^{\mathrm{N}}$. Let $\mathbf{x} = [\mathbf{p}^T \quad \mathbf{Q}^T]^T \in \mathcal{T}$ be the generalized pose of the end-effector, with $\mathcal{T} = \mathbb{R}^3 \times \mathbb{S}^3$, expressed as a combination of the position $\mathbf{p}$ and the orientation in the form of unit $\mathbf{Q}$ (quaternion preliminaries can be found in Appendix A). The mapping between the generalized velocity $\mathbf{v} = [\dot{\mathbf{p}}^T \quad \boldsymbol{\omega}^T]^T$ of the end-effector with $\dot{\mathbf{p}}$, $\boldsymbol{\omega}$ being the translational and angular velocities respectively and $\dot{\mathbf{x}}$ is

$$\dot{\mathbf{x}} = \mathbf{J}_x(\mathbf{x})\mathbf{v}, \tag{1}$$

where $\mathbf{J}_x = \mathrm{diag}\left(\mathbf{I}_3\ ,\ \frac{1}{2}\mathbf{J}_{\mathbf{Q}}\right) \in \mathbb{R}^{7\times 6}$, with $\mathbf{J}_{\mathbf{Q}}$ being the matrix, mapping the angular velocity of the frame to the unit quaternion rates of $\mathbf{Q}$ (see Appendix A-(31)) and $\mathbf{v} = \mathbf{J}(\mathbf{q})\dot{\mathbf{q}}$, where $\mathbf{J}(\mathbf{q}) \in \mathbb{R}^{6\times \mathrm{N}}$ is the robot Jacobian, mapping the velocity of the joints to the end-effector velocity.

The notion of "Partially known task" refers to the subset $\mathcal{S}$ of the task space $\mathcal{T}$, which includes any potential oriented path required to complete the task. Subset $\mathcal{S}$ depends on the uncertainty involved in this knowledge. Furthermore, the temporal properties of the task are considered unknown.

In many cases the partially known task can be mathematically modeled by parameterized expressions $\mathbf{p}_d(\boldsymbol{\sigma}) = [p_d^x(\boldsymbol{\sigma})\ p_d^y(\boldsymbol{\sigma})\ p_d^z(\boldsymbol{\sigma})]^T \in \mathbb{R}^3$ for the position and $\mathbf{Q}_d(\sigma) = [\eta_d(\boldsymbol{\sigma})\ \ \boldsymbol{\epsilon}_d(\boldsymbol{\sigma})^T]^T \in \mathbb{S}^3$ for the orientation, both parameterized by $\boldsymbol{\sigma} = [\sigma_1\ \sigma_2\ ...\sigma_{\mathrm{m}}]^T \in \mathbb{R}^{\mathrm{m}}$ with $\mathrm{m} \leq 6$ denoting the minimum number of parameters required to describe the task. Therefore

$$\mathbf{x}_d(\boldsymbol{\sigma}) = \begin{bmatrix} \mathbf{p}_d(\boldsymbol{\sigma}) \\ \mathbf{Q}_d(\boldsymbol{\sigma}) \end{bmatrix} \in \mathcal{T}, \tag{2}$$

describes the desired end-effector poses , for a given $\boldsymbol{\sigma}$. Notice that (2) implies in general a coupling between position and orientation variables. There have been previous works that utilize the coupling between position and orientation within the scope of learning and autonomously execute synchronized operations, e.g. [58], which refers to asymmetrical bimanual tasks. In this work, we consider hyperrectangles in the parametric space, i.e., $\sigma_i, i = 1\ldots\mathrm{m}$ is bounded $\underline{\sigma}_i < \sigma_i < \overline{\sigma}_i$, with $\underline{\sigma}_i$, $\overline{\sigma}_i \in \mathbb{R}$ being the lower and upper bounds of σ_i respectively and define the set of desired end-effector poses as follows:

$$\mathcal{S} \triangleq \{\mathbf{x}_d(\boldsymbol{\sigma}) \in \mathcal{T} : \underline{\sigma}_i < \sigma_i < \overline{\sigma}_i, \forall i = 1, ..., \mathrm{m}\}. \tag{3}$$

To enhance clarity, in what follows, examples of industrial tasks with their respective parametrization are provided, which differ with respect to the number of degrees-of-freedom (dof) and the level of coupling between position and orientation.

Example II.1. *Surface cutting (1-D curve).*

Consider a cutting task in which the actual cutting curve is known. In this task, every point on the curve corresponds to a specific orientation of the cutting tool. Hence, both position and orientation can be parameterized utilizing a single parameter σ_1, (i.e. $\mathbf{p}_d(\sigma_1)$ and $\mathbf{Q}_d(\sigma_1)$). The limits $\underline{\sigma}_1, \overline{\sigma}_1$ reflect the starting and ending poses of the parameterized curve respectively. Notice that position is fully coupled with orientation in this case, as they both depend on σ_1.

In particular, this 1D curve can be given as a sequence of K key-frames denoted by $\tilde{\mathbf{x}}_{di}$, with $i = 1, ..., \mathrm{K}$. It is possible to find an analytic expression $\mathbf{x}_d(\boldsymbol{\sigma})$ in which $\mathbf{x}_d(\boldsymbol{\sigma}_i) = \tilde{\mathbf{x}}_{di}, \forall i = 1, ..., \mathrm{K}$. One way to achieve this, is by constructing a sequence of Bezier functions $\mathbf{x}_{di}$, where the continuity is preserved in both the path and its tangential vector, in which case the following hold: $\mathbf{x}_{d,i}(\boldsymbol{\sigma}_{i+1}) = \mathbf{x}_{d,i+1}(\boldsymbol{\sigma}_{i+1})$ and $\left.\frac{\partial \mathbf{x}_{d,i}}{\partial \boldsymbol{\sigma}}\right|_{\boldsymbol{\sigma}=\boldsymbol{\sigma}_{i+1}} = \left.\frac{\partial \mathbf{x}_{d,i+1}}{\partial \boldsymbol{\sigma}}\right|_{\boldsymbol{\sigma}=\boldsymbol{\sigma}_{i+1}}, \forall i = 1, ..., \mathrm{K}-1$. A Bezier equivalent in orientation could be provided utilizing either the traditional SQUAD method or the Hermite interpolation, which is based on smooth blending of two great circular arcs in $\mathrm{SO}(3)$, taking into account the tangent vector in every point of the path on $\mathbb{S}^3$ [59], which is the 3 dimensional sphere where unit quaternions belong.

Example II.2. *Milling along a path on a curved surface.*

Consider a milling task along a curved path, in which the human should physically guide a robot, which has a milling tool. In this task, every point on the curve corresponds to a specific orientation of the tool, but any orientation around the normal to the cutting surface should be allowed (Fig.1a), since it does not affect the task. This fact introduces a redundant degree of freedom in orientation. Hence, position can be parameterized as $\mathbf{p}_d(\sigma_1)$ and orientation as

$$\mathbf{Q}_d(\sigma_1, \sigma_2) = \mathbf{Q}_0(\sigma_1)\cos(\pi\sigma_2) + \mathbf{J}_{\mathbf{Q}_0}\mathbf{n}(\sigma_1)\sin(\pi\sigma_2),$$

with $\mathbf{n}(\sigma_1) \in \mathbb{R}^3$ being the normal to the surface and σ_2 the angle around $\mathbf{n}(\sigma_1)$. Notice that, for a given σ_1, $\mathbf{Q}_0(\sigma_1)$ is one allowable orientation and $\mathbf{Q}_d(\sigma_1, \sigma_2)$ represents a geodesic circle of the unit quaternion sphere, since it is the intersection between the vector space of $[\mathbf{Q}_0 \quad \mathbf{J}_{\mathbf{Q}_0}\mathbf{n}(\sigma_1)]$ and the quaternion sphere (Appendix A).In this case $\mathbf{Q}_0$ represents an orientation lying on the geodesic circle, with rotation matrix:

$$\mathbf{R}_0(\sigma_1) = [\boldsymbol{\xi}(\sigma_1) \times \mathbf{n}(\sigma_1) \quad \boldsymbol{\xi}(\sigma_1) \quad \mathbf{n}(\sigma_1)],$$

with $\boldsymbol{\xi}(\sigma_1) = \frac{\frac{\partial \mathbf{p}_d(\sigma_1)}{\partial \sigma_1}}{\|\frac{\partial \mathbf{p}_d(\sigma_1)}{\partial \sigma_1}\|}$.

The limits $\underline{\sigma}_1$ and $\overline{\sigma}_1$ reflect the starting and ending poses of the parameterized curve respectively and the limits of σ_2 can be selected to be $\underline{\sigma}_2 = 0$, $\overline{\sigma}_2 = 1$, to allow a full rotation around $\mathbf{n}(\sigma_1)$.

Example II.3. *Engraving on a 3D surface generated by a rotation of a planar curve.*

Let us consider a case of a surface produced by rotating a 1D planar curve $\mathbf{f}(\sigma_1) \in \mathbb{R}^3$ around an axis $\mathbf{k}$ (Fig.1b). Hence, the surface of the object can be described as

$$\mathbf{p}_d(\sigma_1, \sigma_2) = \mathbf{R}(\mathbf{k}, \sigma_2)\mathbf{f}(\sigma_1),$$

where $\mathbf{R}(\mathbf{k}, \sigma_2) \in \mathbb{R}^{3\times 3}$ is the rotation matrix and σ_2 the a rotation angle. To engrave the object's surface, the engraving

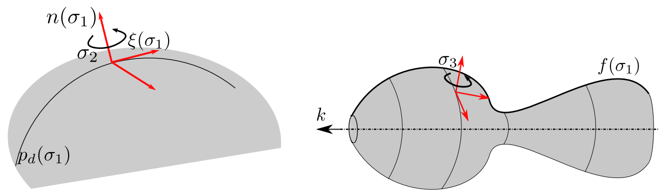

(a) (b)

Fig. 1: Examples II.2 and II.3. a) Milling along the path $\mathbf{p}_d(\sigma_1)$ on curved surface, b) Engraving an object produced by rotating a planar curve.

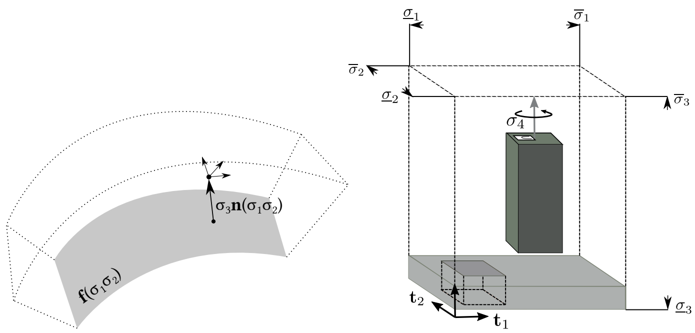

(a) (b)

Fig. 2: Examples II.4 and II.5. a) Motion in a constrained 3-D space, b) Rectangular peg in a hole.

tool should remain perpendicular to the surface. Therefore, there is a coupling between desired position and orientation that rely on σ_1,σ_2. Hence, the desired orientation could be parameterized as $\mathbf{Q}_d(\sigma_1, \sigma_2, \sigma_3)$ with σ_3 being a redundant degree of freedom representing a rotation around the vector normal to the surface, similarly to Example II.2. The limits of σ_1 reflect the starting and ending point of the surface along $\mathbf{f}(\sigma_1)$, those of σ_2 for a surface derived by a full rotation of $\mathbf{f}(\sigma_1)$ can be set to $\underline{\sigma}_2 = -\pi$ and $\overline{\sigma}_2 = \pi$, and those of σ_3 can be set to $\underline{\sigma}_3 = 0$, $\overline{\sigma}_3 = 1$ to allow a full rotation around the normal.

Example II.4. *Tool motion in a unilaterally constrained 3-D space.*

Consider a task, in which the motion should be constrained so that it does not penetrate a surface, while the orientation is totally free, as shown in Fig.2a. Let us a assume that the surface is parameterized as $\mathbf{f}(\sigma_1, \sigma_2) \in \mathbb{R}^3$. Hence, the desired position can be described as

$$\mathbf{p}_d(\sigma_1, \sigma_2, \sigma_3) = \mathbf{f}(\sigma_1, \sigma_2) + \sigma_3\mathbf{n}(\sigma_1, \sigma_2),$$

where $\mathbf{n}$ is the normal to the surface vector and $\sigma_3 > \underline{\sigma}_3 = 0$ to constrain the motion above the surface. The desired orientation in this task is parameterized as $\mathbf{Q}_d(\sigma_4, \sigma_5, \sigma_6)$, representing the whole $\mathbb{S}^3$ space. The bounds of σ_1, σ_2 should reflect the boundaries of the surface $\mathbf{f}(\sigma_1, \sigma_2)$, that of σ_3 should represent the maximum allowable deviation from the surface, and bounds of $\sigma_4, \sigma_5, \sigma_6$ should be selected such that $\mathbf{Q}_d(\sigma_4, \sigma_5, \sigma_6)$ covers the whole $\mathbb{S}^3$.

Example II.5. *Rectangular peg in a hole*

TABLE I: Representative examples and coupling between position and orientation.

Example	$\mathbf{p}_d$	$\mathbf{Q}_d$	Coupling
II.1	$\mathbf{p}_d(\sigma_1)$	$\mathbf{Q}_d(\sigma_1)$	σ_1
II.2	$\mathbf{p}_d(\sigma_1)$	$\mathbf{Q}_d(\sigma_1, \sigma_2)$	σ_1
II.3	$\mathbf{p}_d(\sigma_1, \sigma_2)$	$\mathbf{Q}_d(\sigma_1, \sigma_2, \sigma_3)$	σ_1, σ_2
II.4	$\mathbf{p}_d(\sigma_1, \sigma_2, \sigma_3)$	$\mathbf{Q}_d(\sigma_4, \sigma_5, \sigma_6)$	-
II.5	$\mathbf{p}_d(\sigma_1, \sigma_2, \sigma_3)$	$\mathbf{Q}_d(\sigma_4)$	-

Consider an industrial task, in which the human guides the robot's end-effector grasping a polyhedral peg, with the purpose of inserting it in a hole, as shown in Fig. 2b. Perception errors do not allow precise knowledge of the hole's pose in the working surface of the robot.

In that case, the desired parameterized positions for the task can be described as

$$\mathbf{p}_d(\sigma_1, \sigma_2, \sigma_3) = \mathbf{t}_1\sigma_1 + \mathbf{t}_2\sigma_2 + (\mathbf{t}_1 \times \mathbf{t}_2)\sigma_3,$$

where $\mathbf{t}_1, \mathbf{t}_2 \in \mathbb{R}^3$ are the plane's coordinate axis. By imposing the bounds $\underline{\sigma}_1 < \sigma_1 < \overline{\sigma}_1$, $\underline{\sigma}_2 < \sigma_2 < \overline{\sigma}_2$, $\underline{\sigma}_3 < \sigma_3 < \overline{\sigma}_3$, a space including the hole and the space above the upper surface of the plane can be defined (Fig.2b). Additionally the desired orientation can be described as

$$\mathbf{Q}_d(\sigma_4) = \mathbf{Q}_0 \cos(\pi\sigma_4) + \mathbf{J}_{\mathbf{Q}_0}(\mathbf{t}_1 \times \mathbf{t}_2) \sin(\pi\sigma_4),$$

where σ_4 is a redundant degree of freedom representing a rotation around the normal vector to the surface and $\mathbf{Q}_0$ is the quaternion that describes the orientation of the frame $\mathbf{R}_0 = [\mathbf{t}_1 \;\; \mathbf{t}_2 \;\; \mathbf{t}_1 \times \mathbf{t}_2]$. The limits of σ_4 can be set to $\underline{\sigma}_4 = 0$, $\overline{\sigma}_4 = 1$, similarly to Example II.2, to allow a full rotation around the axis normal to $\mathbf{t}_1$ and $\mathbf{t}_2$.

Table I summarizes the representative examples with the couplings between position and orientation.

III. Problem Description

When the robot is under human guidance, knowledge of the parameterized desired pose $\mathbf{x}_d(\boldsymbol{\sigma})$ can be exploited by the pHRI controller to assist the user in its task. To solve the problem we propose to confine the distance of the current end-effector pose to the desired pose within a predefined set, yielding translational and orientation deviations less than prespecified amounts. As the desired pose is a parameterized function (see Section II), the closest desired pose to the current end-effector pose should be determined. Constraining the distance to the closest desired pose is satisfied by the action of a controller, designed to guarantee that the boundaries of the predefined residual set will not even be reached. Acting on a gravity compensated robot, the produced control input should additionally preserve the passivity between the human interaction force and the end-effector velocity and achieve the boundedness of all signals in the closed-loop system.

Summarizing, the main problem can be split in the following sub-problems:

1) Given the current end-effector pose and the parameterized desired task, find the closest desired pose and calculate the distance of the current to the desired pose.

2) Utilizing the distance of the current to the closest desired pose and a predefined residual set, design a controller to achieve the following objectives: (a) the formulated closed-loop system is strictly output passive with respect to the end-effector velocity, under the exertion of a generalized force imposed by the human guidance; (b) the distance of the current end-effector pose to the closest desired one is constrained to evolve strictly within a predefined (according to constraints) set; (c) all closed-loop signals are bounded.

Remark 1. To guarantee the collaboration of the solutions of the two sub-problems described above, it is mandatory to operate on different time-scales. Specifically, the closest desired pose should be determined significantly faster, compared to the duty-cycle of the control-loop. This is clearly accomplished whenever an analytic solution is available; in all other cases, it is achievable when the problem is locally convex since a general optimization algorithm can be utilized to yield a sufficiently accurate local minimum within one control cycle.

IV. The closest desired pose

In this section the distance of the current end-effector pose $\mathbf{x} = [\mathbf{p}^T \;\; \mathbf{Q}^T]^T \in \mathcal{T}$ to the nearest desired pose is defined.

Notice that in the case of position, the shortest path between two points is a straight line, while in case of orientation the shortest path between two points on the unit quaternion sphere is the minor arc in $\mathbb{S}^3$ which passes through these points (Appendix A).Hence the minor arc is analogous to straight lines in Euclidean geometry.

In that direction, let

$$\mathbf{e}_p(\mathbf{p}, \boldsymbol{\sigma}) = \mathbf{p} - \mathbf{p}_d(\boldsymbol{\sigma}) \tag{4}$$

be the translational error for some σ (i.e., from some position in the parametric task) and

$$\begin{aligned}\mathbf{Q}_e(\mathbf{Q}, \boldsymbol{\sigma}) &= \mathbf{Q} * \mathbf{Q}_d(\boldsymbol{\sigma})^{-1} = [\eta_e(\mathbf{Q}, \boldsymbol{\sigma}) \;\; \boldsymbol{\epsilon}_e(\mathbf{Q}, \boldsymbol{\sigma})^T]^T \\ &= [\cos(\vartheta_e/2) \;\; \sin(\vartheta_e/2)\mathbf{k}_e^T]^T\end{aligned} \tag{5}$$

be the orientation error for some $\boldsymbol{\sigma}$ (i.e., from some orientation in the parametric task), which describes the rotation needed to align $\mathbf{Q}_d(\boldsymbol{\sigma})$ with $\mathbf{Q}$, with $\vartheta_e(\mathbf{Q}, \boldsymbol{\sigma}) \in (-\pi, \pi)$, $\mathbf{k}_e(\mathbf{Q}, \boldsymbol{\sigma})$ being the angle and unit axis of rotation respectively, while with "$*$" the quaternion product (Appendix A) is denoted. Notice that $\eta_e = 1$ if $\mathbf{Q} = \mathbf{Q}_d(\boldsymbol{\sigma})$.

The following metric of the generalized deviation of current pose $\mathbf{x}$ from $\mathbf{x}_d(\boldsymbol{\sigma})$ is proposed:

$$\psi(\mathbf{x}, \boldsymbol{\sigma}) \triangleq \frac{\mathbf{e}_p(\mathbf{p}, \boldsymbol{\sigma})^T \mathbf{e}_p(\mathbf{p}, \boldsymbol{\sigma})}{\mathrm{r_m}^2} + \frac{1 - \eta_e(\mathbf{Q}, \boldsymbol{\sigma})}{1 - \cos{\vartheta_\mathrm{m}/2}}, \tag{6}$$

where $\mathrm{r_m}, \vartheta_\mathrm{m}$ are constant parameters representing prespecified (user defined) bounds on translational and orientational deviation, respectively. In particular $\mathrm{r_m}, \vartheta_\mathrm{m}$ are selected so that $\mathrm{r_m} > \mathrm{r_0} > 0$ and $\pi \geq |\vartheta_\mathrm{m}| > \vartheta_0 > 0$. A similar metric is proposed in [60]. Notice that $\psi(\mathbf{x}, \boldsymbol{\sigma}) = 0$ if $\mathbf{x} = \mathbf{x}_d(\boldsymbol{\sigma})$ and $\psi(\mathbf{x}, \boldsymbol{\sigma}) > 0$ if $\mathbf{x} \neq \mathbf{x}_d(\boldsymbol{\sigma})$. Then,

$$\boldsymbol{\sigma}^*(\mathbf{x}) = \arg\min_{\boldsymbol{\sigma}} \psi(\mathbf{x}, \boldsymbol{\sigma}) \tag{7}$$

corresponds to the minimum deviation $\psi(\mathbf{x}, \boldsymbol{\sigma}^*)$. To simplify notation, $\psi(\mathbf{x}, \boldsymbol{\sigma}^*)$ is from now on denoted as $\psi^*(\mathbf{x})$. Our aim is to guarantee

$$\psi^*(\mathbf{x}) < 1, \tag{8}$$

which implies $0 \leq \frac{\mathbf{e}_p^*(\mathbf{p})^T \mathbf{e}_p^*(\mathbf{p})}{\mathrm{r_m}^2} < 1$ and $0 \leq \frac{1 - \eta_e^*(\mathbf{Q})}{1 - \cos(\vartheta_\mathrm{m}/2)} < 1$, where $\mathbf{e}_p^*(\mathbf{p}) = \mathbf{e}_p(\mathbf{p}, \boldsymbol{\sigma}^*)$ and $\eta_e^*(\mathbf{Q}) = \eta_e(\mathbf{Q}, \boldsymbol{\sigma}^*)$. The latter is equivalent to:

$$\begin{aligned}\|\mathbf{e}_p^*(\mathbf{p})\| &< \mathrm{r_m}, \\ |\vartheta_e(\mathbf{Q}, \boldsymbol{\sigma}^*)| &< \vartheta_\mathrm{m}.\end{aligned} \tag{9}$$

Therefore, the achievement of (8) imposes prescribed (user defined) performance bounds on both the translational and orientation errors. Notice that when $\mathbf{Q} = \mathbf{Q}_d$, the allowable maximum translational deviation is $\mathrm{r_m}$, and respectively when $\mathbf{p} = \mathbf{p}_d$ the allowable maximum deviation in orientation is ϑ_m. In any other case, the maximum allowable deviation in translation and orientation is less than $\mathrm{r_m}$ and ϑ_m, respectively. In general, there is a coupling between the boundaries in translation and orientation since ψ consists of a sum of both metrics. Let

$$\Omega_1 \triangleq \{\mathbf{x} \in \mathcal{T} : \psi^*(\mathbf{x}) < 1\} \tag{10}$$

be the allowable region containing the set of desired end-effector poses $\mathcal{S}$ (i.e., $\mathcal{S} \subset \Omega_1$).Since $\boldsymbol{\sigma}$ is constrained as explained in Section II and illustrated in the examples,(7) can be formalized as the solution of the constrained optimization problem:

$$\begin{aligned}&\underset{\boldsymbol{\sigma}}{\text{minimize}} && \psi(\mathbf{x}, \boldsymbol{\sigma}) \\ &\text{subject to} && \underline{\sigma}_i \leq \sigma_i \leq \overline{\sigma}_i, i = 1, ..., m.\end{aligned} \tag{11}$$

For any sufficiently smooth task, $\psi(\mathbf{x}, \boldsymbol{\sigma})$ is locally convex in a neighborhood of $\boldsymbol{\sigma} \in \mathbb{R}^\mathrm{m}$ with $\sigma_i \in [\sigma_{ci} - \alpha, \sigma_{ci} + \alpha], i = 1, ..., \mathrm{m}$ around any centroid $\boldsymbol{\sigma}_c \in \mathbb{R}^\mathrm{m}$, with $\underline{\sigma}_i \leq \sigma_c \leq \overline{\sigma}_i, i = 1, ..., m$, for some $\alpha > 0$. Notice that such a consideration is not restrictive as any task that does not satisfy this property may equivalently be subdivided into several sufficiently smooth subtasks. Further, we assume that the desired pose $\mathbf{x}_d(\boldsymbol{\sigma})$ is generated before the beginning of the human-robot interaction, so that $\mathbf{x}_d(\boldsymbol{\sigma}_0) = \mathbf{x}_0$, for some $\boldsymbol{\sigma}_0 \in \mathbb{R}^\mathrm{m}$ with $\underline{\sigma}_i \leq \sigma_0 \leq \overline{\sigma}_i, i = 1, ..., m$, with $\mathbf{x}_0$ being the initial end-effector pose, making the initial distance $\psi^*(\mathbf{x})$ zero. Hence, a good choice of $\boldsymbol{\sigma}_c$ for each control cycle $\kappa \in \mathbb{N}$ is the previously found optimal $\boldsymbol{\sigma}_{\kappa-1}^*$ for $\kappa > 0$, and $\boldsymbol{\sigma}_0^* = \boldsymbol{\sigma}_0$ for $\kappa = 0$. If $\sigma_{i,\kappa}^* - \sigma_{i,\kappa-1}^* < \alpha$ for all $\kappa \in \mathbb{N}$ and $i = 1, ..., m$ then owing to the local convexity property, the optimal $\boldsymbol{\sigma}_\kappa^*$ can be determined using any convex constrained optimization algorithm. Therefore, it is possible to get fast a sufficiently accurate local minimum within the control cycle as required by our controller (see Remark 1). Hence, $\psi^*(\mathbf{x})$ is available to the controller for all $t \geq 0$.

In Appendix B it is proven that:

$$\dot{\psi}^*(\mathbf{x}, \mathbf{v}) = \mathbf{v}^T \mathbf{M}_6 \mathbf{e}^*(\mathbf{x}) - \zeta, \tag{12}$$

where $\zeta \triangleq (\mathbf{x} - \mathbf{x}_d(\boldsymbol{\sigma}^*))^T \mathbf{M}_7 \left.\frac{\partial \mathbf{x}_d}{\partial \boldsymbol{\sigma}}\right|_{\boldsymbol{\sigma} = \boldsymbol{\sigma}^*} \dot{\boldsymbol{\sigma}}^*$, with $\zeta \geq 0$ owing to (37), $\mathbf{M}_6 = \mathrm{diag}(\frac{2}{\mathrm{m_p}}\mathrm{I}_3, \frac{1}{2\mathrm{m_o}}\mathrm{I}_3) \in \mathbb{R}^{6\times 6}$, with $\mathrm{m_p} = \mathrm{r_m}^2$, $\mathrm{m_o} = 1 - \cos(\vartheta_\mathrm{m}/2)$ and $\mathbf{e}^*(\mathbf{x}) = [\mathbf{e}_p(\mathbf{p}, \boldsymbol{\sigma}^*)^T \;\; \boldsymbol{\epsilon}_e(\mathbf{Q}, \boldsymbol{\sigma}^*)^T]^T$.

V. Controller design

Let us define the transformed error $\varepsilon \in \mathbb{R}^+$ of ψ^* as

$$\varepsilon \triangleq T\left(\psi^*(\mathbf{x})\right), \tag{13}$$

where $T : [0,1] \rightarrow [0,\infty)$ is any smooth, strictly increasing function, with $T(0) = 0$. A candidate T-function is

$$T(\psi^*(\mathbf{x})) = \ln\left(\frac{1}{1-\psi^*(\mathbf{x})}\right). \tag{14}$$

Differentiating (13) with respect to time it is obtained

$$\dot{\varepsilon} = J_T(\psi^*(\mathbf{x}))\dot{\psi^*}(\mathbf{x}), \tag{15}$$

where $J_T(\psi^*(\mathbf{x})) \triangleq \frac{\partial T}{\partial \psi^*(\mathbf{x})} \in \mathbb{R}^+$. Substituting (12) in (15) yields

$$\dot{\varepsilon} = J_T(\psi^*(\mathbf{x}))\left(\mathbf{v}^T\mathbf{M}_6\mathbf{e}^*(\mathbf{x}) - \zeta\right). \tag{16}$$

The following control force synthesized in the robot's end effector space is proposed:

$$\mathbf{u}_T(\mathbf{x},\mathbf{v}) = -\mathrm{k}T(\psi^*(\mathbf{x}))J_T(\psi^*(\mathbf{x}))\mathbf{M}_6\mathbf{e}^*(\mathbf{x}) - \mathbf{D}\mathbf{v}, \tag{17}$$

where $\mathrm{k} \in \mathbb{R}^+$ is a scalar tunable control parameter and $\mathbf{D} \in \mathbb{R}^{6\times 6}$ a positive definite diagonal matrix, representing the virtual dissipation introduced by the control scheme.

Remark 2. Notice that by selecting an appropriately small gain k one can intensify the non-linearity of term $\mathrm{k}T(\psi^*(\mathbf{x}))$ in (17), resulting in a more flat region when the error is close to the equilibrium and a more steep region when the error is close to the boundary $\psi^*(\mathbf{x}) \equiv 1$. Tuning this gain in a way so that forces generated by the attractive potential in the flat region cannot overcome static friction yields a similar to dissipative control behavior, i.e., the user will not experience any forces when stationary.

Assuming an N-dof non-redundant manipulator, which is compensated for gravity and for which the robot Jacobian $\mathbf{J}(\mathbf{q})$ is invertible and the mapping between the joint space and task space is one-to one, the robot model can be written in task space as follows:

$$\mathbf{\Lambda}_x(\mathbf{x})\dot{\mathbf{v}} + \mathbf{C}_x(\mathbf{x},\mathbf{v})\mathbf{v} = \mathbf{F}_x + \mathbf{u}_T(\mathbf{x},\mathbf{v}), \tag{18}$$

where $\mathbf{\Lambda}_x(\mathbf{x}) = [\mathbf{J}(\mathbf{q})\mathbf{\Lambda}^{-1}(\mathbf{q})\mathbf{J}^T(\mathbf{q})]^{-1}$ and $\mathbf{C}_x(\mathbf{x},\mathbf{v})\mathbf{v} = \mathbf{J}^{-T}(\mathbf{q})\mathbf{C}(\mathbf{q},\dot{\mathbf{q}})\dot{\mathbf{q}} - \mathbf{\Lambda}_x(\mathbf{x})\dot{\mathbf{J}}(\mathbf{q})\dot{\mathbf{q}}$, with $\mathbf{\Lambda}(\mathbf{q}) \in \mathbb{R}^{\mathrm{N}\times\mathrm{N}}$ being the manipulator's inertia matrix, $\mathbf{C}(\mathbf{q},\dot{\mathbf{q}}) \in \mathbb{R}^{\mathrm{N}\times\mathrm{N}}$ the Coriolis and centripetal matrix, $\mathbf{F}_x \in \mathbb{R}^6$ is the external force and torque applied to the end effector by the user. The control signal $\mathbf{u}_T$ is mapped in the joint space by the Jacobian transpose.Notice that the task space inertia matrix $\mathbf{\Lambda}_x$ is positive definite and the matrix $\dot{\mathbf{\Lambda}}_x - 2\mathbf{C}_x$ is skew symmetric. Employing (17) in (18) we get

$$\mathbf{\Lambda}_x(\mathbf{x})\dot{\mathbf{v}} + \{\mathbf{C}_x(\mathbf{x},\mathbf{v}) + \mathbf{D}\}\mathbf{v} + \mathrm{k}J_T T(\psi^*)\mathbf{M}_6\mathbf{e}^* = \mathbf{F}_x. \tag{19}$$

Define the state vector $\mathbf{s} = [\mathbf{v}^T\ \mathbf{x}^T\ \varepsilon]^T \in (\mathbb{R}^6 \times \mathcal{T} \times \mathbb{R})$; the closed-loop system (19), (16) and (1) is written in compact form:

$$\dot{\mathbf{s}} = \mathbf{h}(\mathbf{s},\mathbf{F}_x),$$

where

$$\mathbf{h}(\mathbf{s},\mathbf{F}_x) = \begin{bmatrix} \mathbf{\Lambda}_x^{-1}(-\mathbf{C}_x\mathbf{v} + \mathbf{F}_x + \mathbf{u}_T(\mathbf{x},\mathbf{v})) \\ \mathbf{J}_x\mathbf{v} \\ J_T(\psi^*(\mathbf{x}))\mathbf{v}^T\mathbf{M}_6\mathbf{e}^*(\mathbf{x}) \end{bmatrix}, \tag{20}$$

with $\mathbf{u}_T(\mathbf{x},\mathbf{v})$ being the control signal defined in (17).

Theorem 1. Consider the initial value problem

$$\dot{\mathbf{s}} = \mathbf{h}(\mathbf{s},\mathbf{F}_x),\ \mathbf{s}(t_0) = \mathbf{s}_0 \in \Omega \tag{21}$$

where $\Omega = \mathbb{R}^6 \times \Omega_1 \times \mathbb{R}$, with $\mathbf{h}(\mathbf{s},\mathbf{F}_x)$ as defined in (20) and Ω_1 as defined in (10). The following statements hold:

(i) Under the exertion of an external input $\mathbf{F}_x$ of bounded energy, the system (21) is strictly output passive with respect to $\mathbf{v}$, the state $\mathbf{s}$ is bounded and $\mathbf{x}$ does not escape Ω_1, i.e., $\psi^*(\mathbf{x}(t)) < 1, \forall t \in [t_0,\infty)$.

(ii) For $\mathbf{F}_x = \mathbf{0}_6$, the solution of (21) converges to the equilibrium $\mathbf{s}_d = [\mathbf{0}_6\ \mathbf{x}_d\ 0]^T$ where $\mathbf{x}_d \in \mathcal{S}$, with $\mathcal{S}$ defined in (3).

Proof. (i) By definition $\mathbf{h}(\mathbf{s},\mathbf{F}_x(t))$ is continuous in t and locally Lipschitz with respect to $\mathbf{s}$. Owing to Theorem 3.1 of [61], there exists a time instance $\tau > t_0$,, such that (21) has a unique solution in a maximal time interval $[t_0,\tau)$ with $\tau \in (t_0,\infty)$, i.e., $\mathbf{s}(t) \in \Omega$ for all $t \in [t_0,\tau)$. Consider the following candidate Lyapunov-like function:

$$V = \frac{1}{2}\mathbf{v}^T\mathbf{\Lambda}_x(\mathbf{q})\mathbf{v} + \frac{1}{2}\mathrm{k}\varepsilon^2. \tag{22}$$

Taking its time derivative for all $t \in [t_0,\tau)$, solving (19) with respect to $\mathbf{\Lambda}_x\dot{\mathbf{v}}$ and employing the skew-symmetric property of $\dot{\mathbf{\Lambda}}_x - 2\mathbf{C}_x$ and (16) , $\dot{V}$ becomes

$$\begin{aligned}\dot{V} =& -\mathbf{v}^T\mathbf{D}\mathbf{v} - \mathrm{k}J_T T(\psi^*)\mathbf{v}^T\mathbf{M}_6\mathbf{e}^* \\ &+ \mathrm{k}J_T T(\psi^*)\left(\mathbf{v}^T\mathbf{M}_6\mathbf{e}^* - \zeta\right) + \mathbf{F}_x^T\mathbf{v} \\ \leq& -\underline{\lambda}(\mathbf{D})\mathbf{v}^T\mathbf{v} + \mathbf{F}_x^T\mathbf{v},\end{aligned} \tag{23}$$

where $\underline{\lambda}(\mathbf{D}) \in \mathbb{R}$ denotes the minimum eigenvalue of $\mathbf{D}$. To derive (23) we have further utilized the fact that $\mathrm{k}J_T T(\psi^*)\zeta \geq 0$. Hence, (21) is strictly output passive for all $t \in [t_0,\tau)$, with respect to $\mathbf{v}$ [61]. By completing the squares in (23), we get:

$$\begin{aligned}\dot{V} \leq& -\|\sqrt{\mathbf{D}}\mathbf{v} - \frac{1}{2}\sqrt{\mathbf{D}}^{-1}\mathbf{F}_x\|^2 + \frac{1}{4}\mathbf{F}_x^T\mathbf{D}^{-1}\mathbf{F}_x \\ \leq& \frac{1}{4}\mathbf{F}_x^T\mathbf{D}^{-1}\mathbf{F}_x, \forall t \in [t_0,\tau).\end{aligned} \tag{24}$$

Integrating (24), we get:

$$V(t) \leq V(t_0) + \int_{t_0}^{t}\frac{1}{4}\mathbf{F}_x^T\mathbf{D}^{-1}\mathbf{F}_x, \forall t \in [t_0,\tau]. \tag{25}$$

The integral term of (25) is bounded, owing to the fact that $\mathbf{F}_x$ is of bounded energy, as it represents the force applied by the human to guide the robot. Thus, ε, $\mathbf{v}$ are bounded for all $t \in [t_0,\tau)$. Stated otherwise, there exist compact sets $\Omega_\varepsilon, \Omega_{\mathbf{v}}$ such that $\varepsilon(t) \in \Omega_\varepsilon \subset \mathbb{R}$ and $\mathbf{v}(t) \in \Omega_{\mathbf{v}} \subset \mathbb{R}^6$ for all $t \in [t_0,\tau)$. As a consequence, there exists a positive constant $\overline{\varepsilon}$ such that $\frac{1}{2}k\varepsilon^2 \leq \overline{\varepsilon}$, for all $t \in [t_0,\tau)$, which for the logarithmic function defined in (14) yields $\psi^*(\mathbf{x}) < T^{-1}\left(\sqrt{\frac{2}{k}\overline{\varepsilon}}\right) < 1$, for all $t \in [t_0,\tau)$, i.e., $\mathbf{s}(t)$ evolves within a compact subset of Ω for all $t \in [t_0, \tau)$. Finally, using Theorem 3.3 of [61] we can conclude that τ can be extended to ∞.

(ii) Employing LaSalle invariance principle for $\mathbf{F}_x = \mathbf{0}_6$, it is easy to show that the state will converge to $\mathbf{s}_d$, from (23). □

Remark 3. The theoretical analysis above is given for the non-redundant case. However, the passivity property can be preserved in the redundant case by injecting a damping term in the joint space. In particular the proposed controller for the redundant case is given by $\mathbf{u}_q = \mathbf{J}^T(\mathbf{q})\mathbf{u}_T - \mathbf{D}_q\dot{\mathbf{q}}$ with $\mathbf{u}_T$ given by (17) and $\mathbf{D}_q \in \mathbb{R}^{N\times N}$ being a positive diagonal damping matrix. To show passivity in this case we consider the following storage function $V_q(\mathbf{q}, \dot{\mathbf{q}}) = \frac{1}{2}\dot{\mathbf{q}}^T\mathbf{\Lambda}(\mathbf{q})\dot{\mathbf{q}} + \frac{1}{2}\mathrm{k}\varepsilon^2(\mathbf{q})$. It is not difficult to verify that its time derivative satisfies the following inequality $\dot{V}_q \leq -\dot{\mathbf{q}}^T\left(\mathbf{D}_q + \mathbf{J}^T\mathbf{D}\mathbf{J}\right)\dot{\mathbf{q}} + \boldsymbol{\tau}_x^T\dot{\mathbf{q}}$ where $\boldsymbol{\tau}_x = \mathbf{J}^T\mathbf{F}_x$, implying system's passivity.

VI. Experimental Evaluation

To demonstrate the effectiveness of the proposed methodology, two experimental scenarios were tested using the 7-dof KUKA LWR4+ robotic manipulator. The first experimental scenario consists of a surface cutting (similar to Example II.1), while the second is a folding assembly scenario. The proposed methodology was implemented in C++ utilizing the FRI library with control frequency $\mathrm{f_s} = 1000$ Hz.

Two groups of 17 subjects each, participated in the experiments. All participants were instructed to minimize the time of completion and the path distance. Initially every subject was given time to get familiar with each of the two compared methods before running the experiment. In each experiment, the sequence of executing the compared methods was inverted for each subgroup of 8 and 9 participants. The main purpose of the comparative experimental evaluation is to demonstrate the controller's efficiency in terms of cognitive and physical load. Towards this direction, the following two quality metrics were used, common to both experiments: (a) the duration of task completion T_f, which is measured as the time of physical interaction, (b) the total energy transferred (E) from the user to the robot and vice versa during the interaction, which was calculated as $E = \int |\mathbf{v}^T\mathbf{F}_x|$. The utilization of the duration of task completion as an indirect metric of the cognitive load of the user is based on Fitts law [62]:

$$\overline{I}_p = \frac{I_d}{T_f}, \tag{26}$$

where $\overline{I}_p \in \mathbb{R}^+$ [bits/s] is the unknown but constant (within the short duration of the experiments) information capacity of the motor system of the subject and $I_d \in \mathbb{R}^+$ [bits] the information required to be processed for the accomplishment of the task, i.e. the task's difficulty and T_f is the minimum duration required by the specific subject to accomplish the task. The purpose of instructing the subjects to minimize the time of completion ensures that the information process rate will remain close to $\overline{I}_p$ and the total time duration is representative of the task's difficulty I_d. For instance the threading of a needle requires more time than a regular peg-in-a-hole task when executed by the same user, as it is more cognitive demanding.

Fig. 3: The user manipulates the master kuka and the slave kuka is simulated in the Rviz.

A. Cutting Task

Firstly, the proposed methodology is tested in a master-slave setup, in which the user is physically interacting with the master manipulator and the cutting takes place in a virtual environment by the slave manipulator. A 7-dof KUKA LWR4+ arm is used as the master device and a virtual visualization of a similar arm as the slave device (Fig. 3). Both the slave arm and the virtual scene are visualized utilizing Rviz (embedded in ROS framework). The virtual scene includes a spherical surface S_α with center $\mathbf{p}_c = [0.0 \;\; 0.5585 \;\; -0.0869]^T$m and radius is $\mathrm{r} = 0.2\ m$ and a desired position path C_α on it (Fig. 4a). The desired position path is defined as an arc of length $0.2\pi\mathrm{r}$ on the spherical surface (green line in Fig.4a), which can be described, similarly to Example II.1, as:

$$\mathbf{p}_d(\sigma) = \mathbf{p}_c + \mathrm{r}[\mathbf{v}_1\cos(2\pi\sigma) + \mathbf{v}_2\sin(2\pi\sigma)], \tag{27}$$

with $\sigma \in [\underline{\sigma}, \overline{\sigma}] = [0, \;\; 0.125]$, $\mathbf{v}_1 = [0 \;\; 0 \;\; 1]^T$ and $\mathbf{v}_2 = [0.5736 \;\; -0.8192 \;\; 0]^T$. The virtual spherical surface is also simulated as an object with stiffness $\mathrm{K_S} = 2000\ N/m$ along its radius; hence a force feedback is applied to the master manipulator. The desired end-effector orientation is defined by:

$$\mathbf{Q}_d = \begin{bmatrix} \cos(\pi\sigma) \\ -\sin(\pi\sigma)\dfrac{\mathbf{v}_1 \times \mathbf{v}_2}{||\mathbf{v}_1||\;||\mathbf{v}_2||} \end{bmatrix} * \begin{bmatrix} -0.0001 \\ 0.8870 \\ -0.4618 \\ 0 \end{bmatrix}. \tag{28}$$

Notice that the orientation is designed so that the cutting tool attached to the slave arm will always be perpendicular to the surface.

Before the initiation of the experiment, the robotic manipulator moves autonomously to the initial configuration, which is $\mathbf{q}_0 = [90 \;\; -45 \;\; 0 \;\; 90 \;\; 0 \;\; -45 \;\; -35]^T$deg corresponding to the end-effector pose $\mathbf{x}_0 = [\mathbf{p}_0^T \;\; \mathbf{Q}_0^T]^T = [0.0 \;\; 0.5586 \;\; 0.1131 \;\; 0.0001 \;\; 0.8870 \;\; -0.4618 \;\; 0]^T$, which is selected to satisfy $\mathbf{x}_0 = \mathbf{x}_d(0)$; hence $\psi_0 = 0$. The end-effector frame $\{T_C\}$ is considered to be located at the tool's edge (Fig. 4b). For comparison purposes, the full 6-D dissipative control in translation and orientation (DC) [41] was also implemented. Both in this method and the proposed one, the nearest desired pose is found by utilizing the Levenberg-Marquardt optimization algorithm

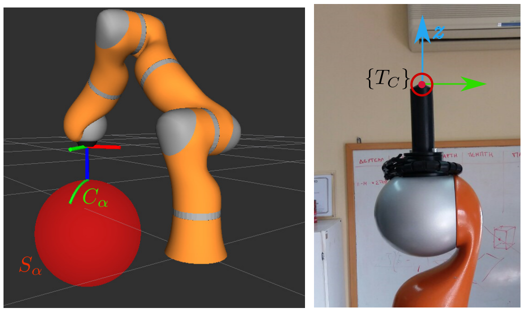

(a) (b)

Fig. 4: (a) Virtual visualization of the virtual slave arm and the virtual scene, (b) frame $\{T_c\}$ in the real robotic arm

with boundary constraints[1] to solve the optimization problem given in equation (11). The proposed method is implemented as given in Remark 3 and the parameters used for the proposed method are: $\vartheta_\mathrm{m} = 5.0^o$, $\mathrm{r_m} = 0.01$m reflecting the task accuracy requirements in position and orientation respectively, $\mathbf{D} = 1.1 I_6$, $\mathrm{k} = 0.5$ and $\alpha = 0.05$ that corresponds to a curve length of ± 6.2cm around the previous nearest point and hence specifies the optimization window at each step. Joint damping parameter $\mathbf{D}_q$ tuning was performed to minimize the user's effort. It was found that the required joint damping injection in this robot is negligible owing to the sufficient inherent joint viscous friction, which is equivalent to a damping injected by the control action. For the DC method the following parameter values were used: $\mathbf{\Sigma}_0 = \mathrm{diag}(4000\mathbf{I}_3\mathrm{N\ m}^{-1}, 3.2\mathbf{I}_3\mathrm{Nm\ rad}^{-1})$, $\mathbf{\Sigma}_1 = \mathrm{diag}(\mathbf{0}_3\mathrm{Ns\ m}^{-1}, \mathbf{0}_3\mathrm{Nms\ rad}^{-1})$, $\mathbf{\Sigma}_2 = \mathrm{diag}(7\mathbf{I}_3\mathrm{Ns\ m}^{-1}, 0.006\mathbf{I}_3\mathrm{Nms\ rad}^{-1})$, $\mathrm{f_c} = 30.0$ N, $\tau_\mathrm{c} = 1.6$ Nm, $\theta = 0.52$ rad. The nomenclature of the parameters of the DC methodology follows the symbolism of [41].

Additional quality metrics regarding the mean absolute error norm from the path in position $\|\mathbf{e}_p\|$ and the mean relative angle of the end-effector from the desired orientation ϑ_e are utilized in this experiment. Boxplots of the statistical results are shown in Fig.5. More specifically, in Fig.5a and 5b the mean position and angle error is depicted, respectively, in which the statistical difference between the proposed method (GAC) and DC is clearly shown, with GAC showing higher accuracy than DC. In particular, the mean error norm in translation is 2.5mm for GAC and 15.8mm for DC, while the mean angular error is 0.03rad and 0.27rad respectively. In Fig.5c and 5d the energy and the total duration are shown, respectively.

A pair-wise t-test was performed to assess whether there is a significant difference between the two methods based on the above defined metrics. Results are shown in Table II. Regarding the mean position error, the angular error and the total energy the proposed controller significantly outperforms the DC method, as indicated by the low p-values (< 0.05). The values of the effect size showing the magnitude of the difference between the two methods in standard deviation units,

[1]http://users.ics.forth.gr/~lourakis/levmar/

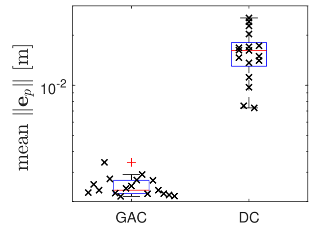

(a) Mean position error with logarithmic vertical axis.

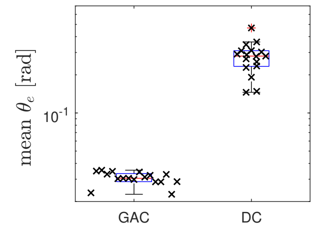

(b) Mean angle error with logarithmic vertical axis.

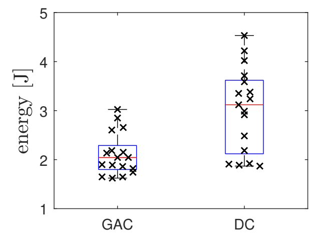

(c) Total energy.

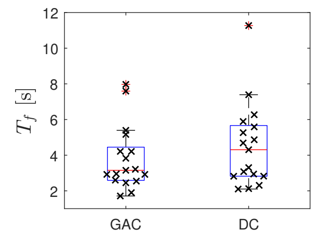

(d) Total duration.

Fig. 5: [Cutting scenario] Boxplots of quality metrics including the distributions of data points with an $\times$-marker.

range from 1.0896 to 3.1739 which could be characterized as large. No such conclusion can be drawn for the total time duration.

TABLE II: t-test results in cutting task scenario

Q. Metric	**result**	**t-stat.**	**d.f.**	**p-value**	**effect size**
mean $\|\|\mathbf{e}_p\|\|$	GAC<DC	-10.63	16	$1.15e^{-8}$	-2.5802
mean θ_e	GAC<DC	-13.08	16	$5.8e^{-10}$	-3.1739
E	GAC<DC	-4.49	16	$3.69e^{-4}$	-1.0896
T_f	-	-1.82	16	0.086	-0.44318

B. Folding assembly task

To validate the applicability and effectiveness of the proposed method in a real task, the case of kinesthetic teaching of the robot for a folding assembly is also tested. More specifically, a two-part folding assembly is considered, between a mobile phone case and a printed circuit board (PCB) (A and B respectively in Fig.6). The PCB is firmly grasped by a two-finger gripper attached to a KUKA LWR4+ manipulator. In this scenario, the phone case is considered static and attached to a supporting surface.

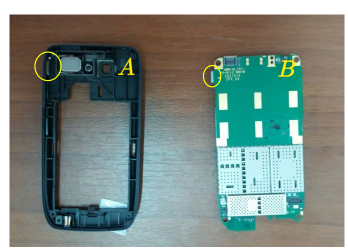

Fig. 6: The assembly parts.

The task requires first the approaching of the PCB towards the case and its contact with it and second the rotation of the

PCB around the contact line, to accomplish a folding motion. Snapshots of the cooperative folding assembly procedure are shown in Fig.7.It is assumed that the contact line (green line in Fig.7) and the supporting surface are known, e.g., they can be identified by robotic vision. To facilitate the insertion of the USB connector into the phone case USB hole (Fig.6, marked in yellow), it is required the PCB to contact the phone case on the contact line with an inclination of 70^o from the supporting surface,as shown in Fig. 7a.Although, it is assumed that both the contact line and the supporting surface are identified with relatively small errors, the opposite is considered for the relative PCB-gripper pose, which may well arise owing to initial grasp error of the PCB or by the slippage of the object during its transfer, as shown in Fig.8.

The task is divided into two phases. In the first phase, the user must guide the robot's end-effector so that the left edge of part B (Fig.6) contacts the left edge of part A from within the case, as shown in Fig.7a-7c and 7f-7h.To accomplish this phase, the PCB's USB connector (marked in yellow in part B of Fig.6) should be inserted into the case USB hole (also marked in yellow in part A of Fig.6). After contact establishment, the second phase is initiated where a rotation of the PCB around the contact line axis (Fig.7c-7e and 7h-7j) is required to accomplish the folding assembly task, as shown in Fig.7e and 7j. To switch from phase 1 to phase 2, an interface with a keyboard input is provided to the user. Each phase is characterized by different desired poses, which are defined as follows.

Phase 1 (Contact).: Owing to the given geometry of the opposing fingers and the planar shape of the PCB, the possible errors are restricted to the PCB plane regarding translation, and around the normal, regarding orientation, as shown in Fig.8. Hence, the desired position is defined as a 2D plane (yellow plane in Fig.7) including the contact line (green line in Fig.7), having an inclination of 70^o from the supporting surface. Such a task-related knowledge could be provided by an expert via an appropriate interface, i.e., an augmented reality graphical user interface in which the user could be able to define the inclination of the plane after the contact line was identified by robotic vision. In this way, the interface would appropriately compute and set the parameters of the analytic expression of the task, according to the selection of the expert.
Therefore, the desired position is described by

$$\mathbf{p}_d(\sigma_1, \sigma_2) = \mathbf{p}_0 + \sigma_1 \mathbf{v} + \sigma_2 \boldsymbol{\lambda},$$

with $\boldsymbol{\lambda} = [1\ 0\ 0]^T$ being the unit vector along the contact line (Fig.7a and 7f), $\mathbf{v} = [0\ \ -0.34\ 0.93]^T$ and $\mathbf{p}_0 = [-0.294\ 0.6308\ 0.167]^T$m. To remain within the workspace of the task we set $\underline{\sigma}_1 = 0, \overline{\sigma}_1 = 2, \sigma_2, \underline{\sigma}_2 = -0.6, \overline{\sigma}_2 = 0.6$.

The desired orientation is described by

$$\mathbf{Q}_d(\sigma_3) = \mathbf{Q}_{gc}(\sigma_3; \mathbf{Q}_{d0}, \mathbf{n}),$$

with $\mathbf{Q}_{gc}$ being the great circle of the quaternion sphere $\mathbb{S}^3$ defined in (35) of Appendix A,$\mathbf{n}$ being the vector normal to the plane $\mathbf{p}_d(\sigma_1, \sigma_2)$ as shown in Fig.7a and $\mathbf{Q}_{d0} = [0.0607\ \ 0.0073\ \ 0.9846\ \ 0.1631]^T$. Notice that $\mathbf{Q}_d(\sigma_3)$ describes a fullrotation around the normal to the surface, thus $\underline{\sigma}_3 = -\pi, \overline{\sigma}_3 = \pi$ are selected.

Prior to experimentation, the robotic manipulator moves autonomously to the initial configuration $\mathbf{q}_0 = [134.248\ \ -73.44\ \ -71.88\ 85.197\ \ 77.4\ \ -54.86\ 52.52]^T$deg with corresponding end-effector pose $\mathbf{x}_0 = [-0.294\ \ 0.6308\ \ 0.167\ \ 0.0607\ \ 0.0073\ \ 0.9846\ \ 0.1631]^T$, which, similarly to the first scenario, was selected to satisfy $\mathbf{x}_0 = [\mathbf{p}_d(0,0)^T\ \ \mathbf{Q}_d(0)^T]^T$.

Notice that in this phase the nearest pose is analytically computable since the parametric expression is decoupled between translation and rotation. Hence, the nearest position is found by projecting the position of the robot to the plane and the nearest orientation is found as explained in Appendix A.

Phase 2.: As shown in Fig.7c-7e, the object has to be rotated around axis $\boldsymbol{\lambda}$. Hence, the desired position can be described by the following arc around the contact line:

$$\mathbf{p}_d(\sigma_1) = \mathbf{p}_\lambda + Rot(\boldsymbol{\lambda}, \sigma_1)(\mathbf{p}_{0b} - \mathbf{p}_\lambda),$$

where $\mathbf{p}_\lambda = [0\ \ 0.69\ \ 0.005]^T$ is an arbitrarily selected point in the contact line and $\mathbf{p}_{0b}$ is the end-effector's position when the phase switches from 1 to 2. The desired orientation can be described by

$$\mathbf{Q}_d(\sigma_1) = \mathbf{Q}_{gc}(\sigma_1; \mathbf{Q}_{0b}, \boldsymbol{\lambda}),$$

with $\mathbf{Q}_{0b}$ being the end-effector orientation when the phase switches from 1 to 2. For this phase the *dlib* library for C++ is utilized with an ending condition of 10^{-19} (slope of solution) and 120 maximum iterations, for the nearest pose search. To ensure that the optimization algorithm will yield a result within one control cycle, we measured the time needed for 120 algorithm iterations for this problem, and found this time being less than our control cycle of 1ms. The parameters used for the proposed method are: $\vartheta_{\mathrm{m}} = 3.0^o$, $\mathrm{r_m} = 0.005$m, $\mathbf{D} = 1.1\mathbf{I}_6$, $k = 0.5$, $\alpha = 0.025$ and $\underline{\sigma}_1 = -\pi, \overline{\sigma}_1 = \pi$.

In this experimental scenario, gravity compensation control mode (GC) is utilized for comparison purposes. The additional quality metrics utilized in this experiment are the path distance in position $d_p = \int_0^{T_f} \|\dot{\mathbf{p}}(t)\| dt$ and orientation $d_o = \int_0^{T_f} \|\boldsymbol{\omega}(t)\| dt$.

Boxplots of the statistical results are shown in Fig.9. More specifically, in Fig.9a and 9b the path distances traveled in position and orientation are depicted, respectively, in which the statistical difference between the proposed method (GAC) and GC is clearly shown, with GAC yielding a shorter path for the task accomplishment. In Fig.9c and 9d the energy and the total duration are shown, respectively. Let us note that not all users were able to complete the task with GC as it was difficult for them to "imagine" or "find out how" to interact with the robot in their own words for the rotation of the end-effector during phase two. Two of them were given further instructions and managed to complete the task while the other two abandoned the task. In the latter case, the total time of physical interaction before abandoning the task was considered for the statistical analysis.

Similarly to the first experimental scenario, a pair-wise t-test was performed, to assess whether the difference between the two methods is statistically significant, based on the above metrics. The results are given in Table III, based on

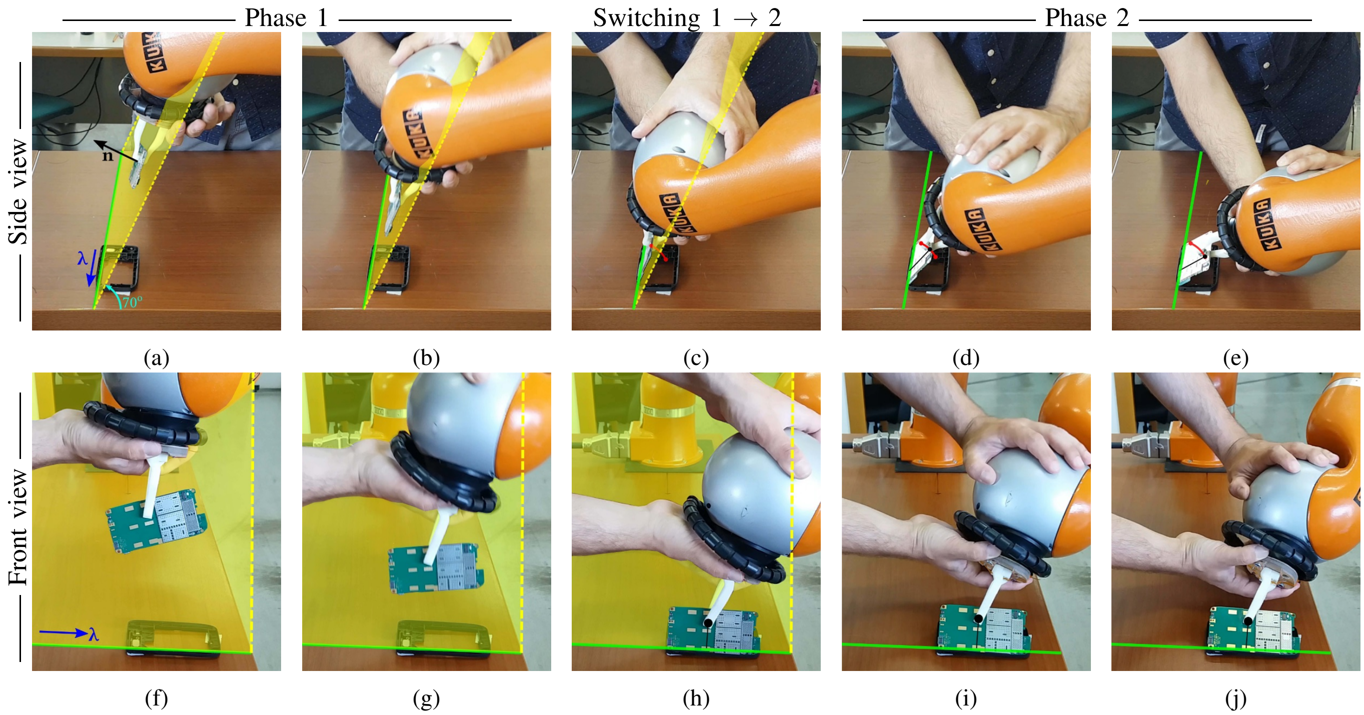

Fig. 7: Snapshots of the folding assembly task.

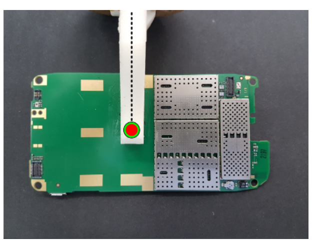

(a) Desired grasp.

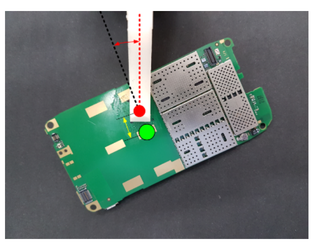

(b) Perturbed grasp.

Fig. 8: Displacement of PCB with respect to the desired grasp. Red dot: gripper's tip center, green dot: desired grasp location, black dashed line: desired **z**-axis of the grasp, red dashed line: **z**-axis of the gripper.

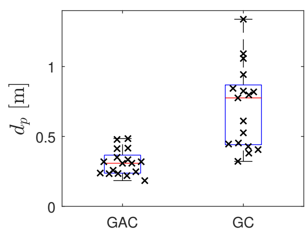

(a) Length of path in position.

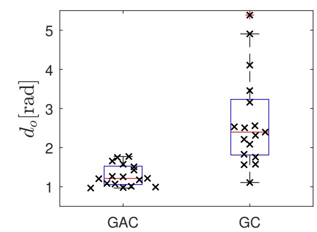

(b) Length of path in orientation.

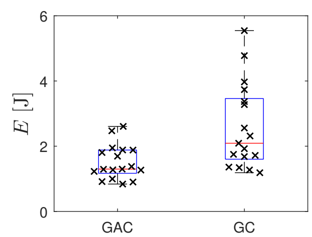

(c) Total energy.

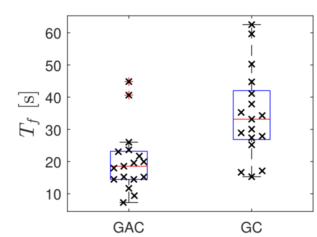

(d) Total duration.

Fig. 9: [Folding scenario] Boxplots of quality metrics including the distributions of data points with an ×-marker.

which we can infer that the mean values of quality metrics differ significantly, with a sufficient level of confidence (p-value below 0.05). Notice that in this application scenario a significant difference in time duration is also found as opposed to the previous scenario, implying the reduction of the difficulty of the task I_d, i.e. the user's cognitive load reduction.

TABLE III: t-test results in folding task scenario

Q. Metric	**result**	**t-stat.**	**d.f.**	**p-value**	**effect size**
d_p	GAC<GC	-6.81	16	$4.13e^{-6}$	-1.6534
d_o	GAC<GC	-5.62	16	$3.83e^{-5}$	-1.3631
E	GAC<GC	-3.67	16	0.002	-0.891981
T_f	GAC<GC	-8.51	16	$2.44e^{-7}$	-2.0655

Fig.10 shows the paths of two representative subjects, which wereequally familiar with both control approaches. Notice the erratic path with the GC controller as opposed to the proposed method, which demonstrates the statistical results based on the path distance d_p, d_o.

VII. Discussion

Given the partial knowledge of the task, the proposed controller enhances the performance of the pHRI task as it was demonstrated in the experimental section; its impact is particularly high for tasks that cannot be accomplished by naive users. However, notice that the proposed controller refers to static spatial task knowledge (not explicitly depending on time). Tasks that could for example involve objects placed

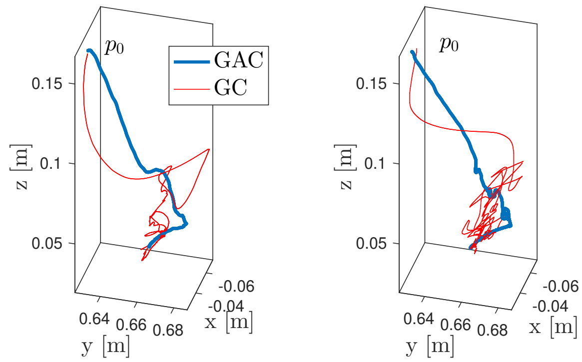

(a) S1 (b) S2

Fig. 10: Translational path of folding assembly task experiment.

on a conveyor belt are not addressed. Moreover, notice that partial knowledge may be associated with uncertainty. In this case, the level of parameterization and the control parameter value selection should reflect this uncertainty, otherwise the suggested controller may slow or even prevent the users from reaching the correct pose. In fact, given an estimate of the maximum uncertainty level, say e.g., in the end-effector position, we can select higher parameter values for $\mathrm{r_m}$, ϑ_m combined with low k values in the controller or introduce a higher degree of parameterization, e.g., in the 1-dof case, instead of an oriented path the task can be modeled as a tube around the nominal 1-dof curve. To evaluate the effectiveness of the proposed method in the presence of perception errors for a given estimated uncertainty, we have performed a series of experiments with the cutting task using the same control parameters, but with the desired oriented path being erroneously defined with respect to the actual (by translating $\mathbf{p}_c$ from 0.2 to 1.5cm in (27) or rotating $\mathbf{v}_1$ from 1 to 5^o around the z-axis in (27) and (28)). Even though the respective plots are not included, the results achieved clearly indicate that both forces and errors are increasing as the unreliability of the constraints increases. However, the user completes the task with less errors when the proposed controller is utilized compared to the ones obtained with the dissipative controller.

VIII. Conclusion

A pHRI controller was proposed, to assist the human user towards achieving a multi degrees of freedom task, for which partial knowledge is available. The proposed approach utilizes a parameterized task model and develops a torque control signal, according to the prescribed performance control methodology. The resulted closed-loop system is proven strictly output passive with respect to the end-effector velocity and it is shown that the translational and orientation deviations are kept less than certain prespecified values. Furthermore, two experimental cases, involving a group of subjects, are conducted with the help of a KUKA LWR4+ robot, showing that the proposed control scheme outperforms the dissipative control, as well as the gravity compensation control mode both in terms of total time and energy.

Appendix A
Unit Quaternion Preliminaries

Given a rotation matrix $\mathbf{R} \in SO(3)$, an orientation can be expressed in terms of the unit quaternion $\mathbf{Q} \in \mathbb{S}^3$ as $\mathbf{Q} = [\eta \ \boldsymbol{\epsilon}^T]^T$, where $\eta \in \mathbb{R}$, $\boldsymbol{\epsilon} \in \mathbb{R}^3$ and $\eta^2 + \boldsymbol{\epsilon}^T\boldsymbol{\epsilon} = 1$. In fact, $\eta = \cos\left(\frac{\vartheta}{2}\right)$ and $\boldsymbol{\epsilon} = \sin\left(\frac{\vartheta}{2}\right)\mathbf{k}$, for the equivalent axis $\mathbf{k} \in \mathbb{R}^3$ ($||\mathbf{k}|| = 1$) and angle ϑ derived from $\mathbf{R}$.

Vice versa, given a unit quaternion $\mathbf{Q} \in \mathbb{S}^3$ we can extract the corresponding rotation $\mathbf{R} = Rot(\mathbf{k}, \vartheta) \in SO(3)$, where $\vartheta = 2\cos^{-1}(\eta)$ and

$$\mathbf{k} = \begin{cases} \frac{\boldsymbol{\epsilon}}{\sin\left(\frac{\vartheta}{2}\right)} & \text{if } \vartheta \neq j\pi, \ j = 0, 1, \ldots \\ 0 & \text{otherwise} \end{cases}.$$

The inverse unit quaternion $\mathbf{Q}^{-1} \in \mathbb{S}^3$ is given by $\mathbf{Q}^{-1} = [\eta \ -\boldsymbol{\epsilon}^T]^T$ and corresponds to the inverse rotation $Rot(\mathbf{k}, -\vartheta)$.

The quaternion product,"$*$", for two given $\mathbf{Q}_1$ and $\mathbf{Q}_2 \in \mathbb{S}^3$ corresponding to the rotation matrices $\mathbf{R}_1$ and $\mathbf{R}_2$ respectively, is defined as follows:

$$\mathbf{Q}_2 * \mathbf{Q}_1 = \begin{bmatrix} \eta_1 & -\boldsymbol{\epsilon}_1^T \\ \boldsymbol{\epsilon}_1 & \eta_1\mathbf{I}_3 - \mathbf{S}(\boldsymbol{\epsilon}_1) \end{bmatrix} \mathbf{Q}_2 \quad \in \mathbb{S}^3, \tag{29}$$

where $\mathbf{S}(.)$ denotes the skew symmetric matrix. Equation (29) expresses consecutive rotations in the same order as rotation matrices do, $\mathbf{R}_2\mathbf{R}_1$.

The time derivative of the quaternion can be related to the angular velocity vector $\boldsymbol{\omega}$ as follows:

$$\dot{\mathbf{Q}} = \frac{1}{2}\mathbf{J_Q}\boldsymbol{\omega}, \tag{30}$$

where

$$\mathbf{J_Q} = \begin{bmatrix} -\boldsymbol{\epsilon}^T \\ \eta\mathbf{I}_3 - \mathbf{S}(\boldsymbol{\epsilon}) \end{bmatrix}. \tag{31}$$

The columns of $\mathbf{J_Q}$ form an orthogonal base of the hyperplane tangential to the unit quaternion sphere at $\mathbf{Q}$. Hence $\mathbf{J_Q^T}\mathbf{J_Q} = \mathbf{I}_{3\times3}$ and $\mathbf{J_Q^T}\mathbf{Q} = \mathbf{0}_{3\times1}$ [see e.g. [63], [64]].

If $\mathbf{Q}_d$ denotes the desired rotation matrix of the end- effector frame and $\mathbf{Q}_c$ the current orientation, the orientation error between two frames can be expressed in terms of quaternions as: $\mathbf{Q}_e = \mathbf{Q}_c * \mathbf{Q}_d^{-1}$. Let $\mathbf{Q}_e = [\eta_e \ \boldsymbol{\epsilon}_e^T]^T$. Hence,

$$\begin{aligned} \eta_e &= \eta_c\eta_d + \boldsymbol{\epsilon}_d^T\boldsymbol{\epsilon}_c = \mathbf{Q}_c^T\mathbf{Q}_d \\ \boldsymbol{\epsilon}_e &= -\eta_c\boldsymbol{\epsilon}_d + \eta_d\boldsymbol{\epsilon}_c + \boldsymbol{\epsilon}_d \times \boldsymbol{\epsilon}_c. \end{aligned} \tag{32}$$

It is noteworthy that

$$\boldsymbol{\epsilon}_e = \mathbf{J}_{\mathbf{Q}_d}^T(\mathbf{Q}_c - \mathbf{Q}_d). \tag{33}$$

By differentiating η_e from (32) and utilizing (33), we get:

$$\dot{\eta}_e = -\frac{1}{2}\boldsymbol{\epsilon}_e^T(\boldsymbol{\omega}_c - \boldsymbol{\omega}_d). \tag{34}$$

Assume an orientation $\mathbf{Q}_o \in \mathbb{S}^3$ and a unit vector $\bar{\boldsymbol{\omega}}_o \in \mathbb{R}^3$ expressing a rotation axis. The great circle determined by the intersection of the unit quaternion sphere and the hyperplane passing from the center and spanned by $\mathbf{Q}_o$ and $\boldsymbol{\delta Q}_o = \mathbf{J_{Q_o}}\bar{\boldsymbol{\omega}}_o$ as shown in Fig. 11, corresponds to two complete rotations of $\mathbf{Q}_o \in \mathbb{S}^3$ around the axis $\bar{\boldsymbol{\omega}}_o$ and is given by the following expression:

$$\begin{aligned}\mathbf{Q}_{gc}(\gamma; \mathbf{Q}_o, \bar{\boldsymbol{\omega}}_o) &= \mathbf{Q}_o \cos(\frac{\gamma}{2}) + \boldsymbol{\delta}\mathbf{Q}_o \sin(\frac{\gamma}{2}) \\ &= \mathbf{Q}_o \cos(\frac{\gamma}{2}) + \mathbf{J}_{\mathbf{Q}_o} \bar{\boldsymbol{\omega}}_o \sin(\frac{\gamma}{2}).\end{aligned} \quad (35)$$

Given any orientation $\mathbf{Q}_1$, it is easy to show that the value of γ which minimizes the geodesic distance between $\mathbf{Q}_1$ and the great circle $\mathbf{Q}_{gc}(\gamma; \mathbf{Q}_o, \bar{\boldsymbol{\omega}}_o)$ can be found analytically from $\gamma^* = 2\text{atan2}(\boldsymbol{\delta}\mathbf{Q}_o^T\mathbf{Q}_1,\ \mathbf{Q}_o^T\mathbf{Q}_1)$, and consequently the closest orientation of the great circle to $\mathbf{Q}_1$ is $\mathbf{Q}_{gc}(\gamma^*; \mathbf{Q}_o, \bar{\boldsymbol{\omega}}_o)$.

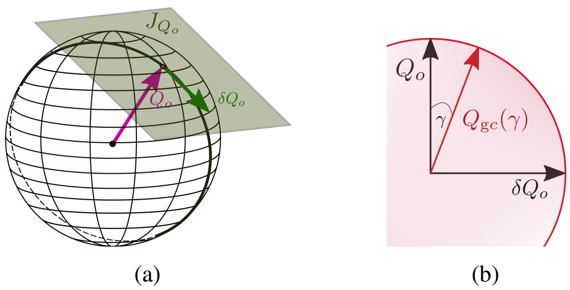

Fig. 11: (a) The tangential hyperplane touches the unit sphere $\mathbb{S}^3$ in $\mathbf{Q}_o$. $\boldsymbol{\delta}\mathbf{Q}_o$ is the unit quaternion lying in this hyperplane, (b)The parametric quaternion curve

APPENDIX B
PROOF OF (12)

The following holds at each control cycle for the optimal solution $\boldsymbol{\sigma}^*$: $-(\boldsymbol{\sigma}^*(t) - \boldsymbol{\sigma})^T \left.\frac{\partial \psi}{\partial \boldsymbol{\sigma}}\right|_{\boldsymbol{\sigma}=\boldsymbol{\sigma}^*} \geq 0$, for all $\boldsymbol{\sigma} \in \Omega_\sigma$ [65], where $\Omega_\sigma(\boldsymbol{\sigma}_c) = \{\boldsymbol{\sigma} \in \mathbb{R}^m : \sigma_{ci} - \alpha \leq \sigma_i \leq \sigma_{ci} + \alpha, \forall i = 1, ..., m\}$. Hence, given that both current $\boldsymbol{\sigma}^*(t)$ and the previous $\boldsymbol{\sigma}^*(t - dt)$ solution of the optimization problem (11) belongs to $\Omega_\sigma(\boldsymbol{\sigma}^*(t - dt))$ (due to the selection below (11)), the inequality is satisfied for $\boldsymbol{\sigma} = \boldsymbol{\sigma}^*(t - dt)$, and the following holds for a sufficiently small control cycle dt:

$$-\dot{\boldsymbol{\sigma}}^{*T} \left.\frac{\partial \psi}{\partial \boldsymbol{\sigma}}\right|_{\boldsymbol{\sigma}=\boldsymbol{\sigma}^*} \geq 0. \quad (36)$$

Substituting the partial derivative of (6) in equation (36) and η_e from (32), and utilizing $\mathbf{Q}_d^T \frac{\partial \mathbf{Q}_d}{\partial \boldsymbol{\sigma}} = 0$ yields

$$(\mathbf{x} - \mathbf{x}_d(\boldsymbol{\sigma}^*))^T \mathbf{M}_7 \left.\frac{\partial \mathbf{x}_d}{\partial \boldsymbol{\sigma}}\right|_{\boldsymbol{\sigma}=\boldsymbol{\sigma}^*} \dot{\boldsymbol{\sigma}}^* \geq 0, \quad (37)$$

where $\mathbf{M}_7 = \text{diag}(\frac{2}{\mathrm{m_p}}\mathbf{I}_3, \frac{1}{\mathrm{m_o}}\mathbf{I}_4) \in \mathbb{R}^{7\times7}$ is a constant diagonal matrix. Let us define ζ as:

$$\zeta \triangleq (\mathbf{x} - \mathbf{x}_d(\boldsymbol{\sigma}^*))^T \mathbf{M}_7 \left.\frac{\partial \mathbf{x}_d}{\partial \boldsymbol{\sigma}}\right|_{\boldsymbol{\sigma}=\boldsymbol{\sigma}^*} \dot{\boldsymbol{\sigma}}^*, \quad (38)$$

for which it holds $\zeta \geq 0, \forall t \in [0, \infty)$ from (37).

Taking the time derivative of (6) with $\boldsymbol{\sigma} = \boldsymbol{\sigma}^*$ yields

$$\dot{\psi}^* = 2\frac{\dot{\mathbf{e}}_p^{*T}\mathbf{e}_p^*}{\mathrm{m_p}} - \frac{\dot{\eta}_e^*}{\mathrm{m_o}}, \quad (39)$$

where $\mathbf{e}^* = [\mathbf{e}_p^{*T}\ \ \mathbf{e}_o^{*T}]^T = [\mathbf{e}_p(\mathbf{p}, \boldsymbol{\sigma}^*)^T\ \ \mathbf{e}_o(\mathbf{Q}, \boldsymbol{\sigma}^*)^T]^T$ with $\mathbf{e}_o^*(\mathbf{Q}) = [\eta_e^*\ \ \boldsymbol{\epsilon}_e^{*T}]$. By utilizing (34) we obtain:

$$\dot{\eta}_e^* = -\tfrac{1}{2}(\boldsymbol{\omega} - \boldsymbol{\omega}_d^*)^T \boldsymbol{\epsilon}_e^*. \quad (40)$$

Substituting (40) in (39) yields $\dot{\psi}^* = 2\frac{\dot{\mathbf{e}}_{\mathbf{p}}^{*T}\mathbf{e}_p^*}{\mathrm{m_p}} + \frac{(\boldsymbol{\omega}-\boldsymbol{\omega}_d^*)^T\boldsymbol{\epsilon}_e^*}{2\mathrm{m_o}}$. Utilizing (30), (33) for $\boldsymbol{\omega}_d = \boldsymbol{\omega}_d^*$ and $\boldsymbol{\epsilon}_e = \boldsymbol{\epsilon}_e^*$ respectively, we obtain

$$\dot{\psi}^* = 2\frac{\dot{\mathbf{e}}_{\mathbf{p}}^{*T}\mathbf{e}_p^*}{\mathrm{m_p}} + \frac{\boldsymbol{\omega}^T\boldsymbol{\epsilon}_e^*}{2\mathrm{m_o}} - \frac{\dot{\mathbf{Q}}_d^{*T}\mathbf{J}_{\mathbf{Q}_d^*}\mathbf{J}_{\mathbf{Q}_d^*}^T(\mathbf{Q} - \mathbf{Q}_d^*)}{\mathrm{m_o}}. \quad (41)$$

Since $\dot{\mathbf{Q}}_d^*$ belongs to the column space of $\mathbf{J}_{\mathbf{Q}_d^*}$, it holds $\mathbf{J}_{\mathbf{Q}_d^*}\mathbf{J}_{\mathbf{Q}_d^*}^T\dot{\mathbf{Q}}_d^* = \dot{\mathbf{Q}}_d^*$. Therefore (41) takes the form

$$\dot{\psi}^* = -(\mathbf{x} - \mathbf{x}_d^*)^T\mathbf{M}_7\dot{\mathbf{x}}_d^* + 2\frac{\dot{\mathbf{p}}^T\mathbf{e}_p^*}{\mathrm{m_p}} + \frac{\boldsymbol{\omega}^T\boldsymbol{\epsilon}_e^*}{2\mathrm{m_o}}. \quad (42)$$

Substituting $\dot{\mathbf{x}}_d^* = \frac{\partial \mathbf{x}_d^*}{\partial \boldsymbol{\sigma}^*}\dot{\boldsymbol{\sigma}}^*$ in (42) yields

$$\dot{\psi}^* = -(\mathbf{x} - \mathbf{x}_d^*)^T\mathbf{M}_7\frac{\partial \mathbf{x}_d^*}{\partial \boldsymbol{\sigma}^*}\dot{\boldsymbol{\sigma}}^* + 2\frac{\dot{\mathbf{p}}^T\mathbf{e}_p^*}{\mathrm{m_p}} + \frac{\boldsymbol{\omega}^T\boldsymbol{\epsilon}_e^*}{2\mathrm{m_o}} \quad (43)$$

and by utilizing (38) in (43) we get (12).

REFERENCES

[1] H. Ding, M. Schipper, and B. Matthias, "Optimized task distribution for industrial assembly in mixed human-robot environments - case study on io module assembly," in *2014 IEEE International Conference on Automation Science and Engineering (CASE)*, pp. 19–24, Aug 2014.

[2] A. Cherubini, R. Passama, A. Crosnier, A. Lasnier, and P. Fraisse, "Collaborative manufacturing with physical human–robot interaction," *Robotics and Computer-Integrated Manufacturing*, vol. 40, pp. 1–13, 2016.

[3] L. B. Rosenberg, "The use of virtual fixtures as perceptual overlays to enhance operator performance in remote environments.," tech. rep., DTIC Document, 1992.

[4] O. Khatib, K. Yokoi, O. Brock, K. Chang, and A. Casal, "Robots in human environments: Basic autonomous capabilities," *The International Journal of Robotics Research*, vol. 18, no. 7, pp. 684–696, 1999.

[5] D. Lee and C. Ott, "Incremental kinesthetic teaching of motion primitives using the motion refinement tube," *Autonomous Robots*, vol. 31, no. 2, pp. 115–131, 2011.

[6] N. Hogan, "Impedance control: An approach to manipulation," in *1984 American Control Conference*, pp. 304–313, June 1984.

[7] W. S. Newman, "Stability and performance limits of interaction controllers," *Transactions-American Society of Mechanical Engineers Journal of Dynamic Systems Measurements and Control*, vol. 114, pp. 563–563, 1992.

[8] S. Golz, C. Osendorfer, and S. Haddadin, "Using tactile sensation for learning contact knowledge: Discriminate collision from physical interaction," in *2015 IEEE International Conference on Robotics and Automation (ICRA)*, pp. 3788–3794, May 2015.

[9] A. D. Luca and F. Flacco, "Integrated control for phri: Collision avoidance, detection, reaction and collaboration," in *2012 4th IEEE RAS EMBS International Conference on Biomedical Robotics and Biomechatronics (BioRob)*, pp. 288–295, June 2012.

[10] B. Navarro, A. Cherubini, A. Fonte, R. Passama, G. Poisson, and P. Fraisse, "An ISO10218-compliant adaptive damping controller for safe Physical Human-Robot Interaction," in *ICRA: International Conference on Robotics and Automation*, (Stockholm, Sweden), May 2016.

[11] A. D. Santis, B. Siciliano, A. D. Luca, and A. Bicchi, "An atlas of physical humanâĂŞrobot interaction," *Mechanism and Machine Theory*, vol. 43, no. 3, pp. 253 – 270, 2008.

[12] R. Ikeura and H. Inooka, "Variable impedance control of a robot for cooperation with a human," in *Robotics and Automation, 1995. Proceedings., 1995 IEEE International Conference on*, vol. 3, pp. 3097–3102, IEEE, 1995.

[13] R. Ikeura, T. Moriguchi, and K. Mizutani, "Optimal variable damping control for a robot carrying an object with a human," in *Proceedings of the International Conference on Control*, pp. 2001–10, 2001.

[14] V. Duchaine and C. M. Gosselin, "General model of human-robot cooperation using a novel velocity based variable impedance control," in *EuroHaptics Conference, 2007 and Symposium on Haptic Interfaces for Virtual Environment and Teleoperator Systems. World Haptics 2007. Second Joint*, pp. 446–451, IEEE, 2007.

[15] F. Dimeas and N. Aspragathos, "Learning optimal variable admittance control for rotational motion in human-robot co-manipulation," *IFAC-PapersOnLine*, vol. 48, no. 19, pp. 124–129, 2015.

[16] A. Lecours, B. Mayer-St-Onge, and C. Gosselin, "Variable admittance control of a four-degree-of-freedom intelligent assist device," in *Robotics and Automation (ICRA), 2012 IEEE International Conference on*, pp. 3903–3908, IEEE, 2012.

[17] F. Ficuciello, L. Villani, and B. Siciliano, "Variable impedance control of redundant manipulators for intuitive human–robot physical interaction," *IEEE Transactions on Robotics*, vol. 31, no. 4, pp. 850–863, 2015.

[18] F. Ferraguti, C. T. Landi, L. Sabattini, M. Bonfe, C. Fantuzzi, and C. Secchi, "A variable admittance control strategy for stable physical humanâĂŞrobot interaction," *The International Journal of Robotics Research*, vol. 38, no. 6, pp. 747–765, 2019.

[19] F. Dimeas and N. Aspragathos, "Online stability in human-robot cooperation with admittance control," *IEEE Transactions on Haptics*, vol. 9, pp. 267–278, April 2016.

[20] I. Ranatunga, S. Cremer, D. O. Popa, and F. L. Lewis, "Intent aware adaptive admittance control for physical human-robot interaction," in *2015 IEEE International Conference on Robotics and Automation (ICRA)*, pp. 5635–5640, May 2015.

[21] O. Dermy, F. Charpillet, and S. Ivaldi, "Multi-modal intention prediction with probabilistic movement primitives," in *Human Friendly Robotics* (F. Ficuciello, F. Ruggiero, and A. Finzi, eds.), (Cham), pp. 181–196, Springer International Publishing, 2019.

[22] A. Sidiropoulos, Y. Karayiannidis, and Z. Doulgeri, "Human-robot collaborative object transfer using human motion prediction based on dynamic movement primitives," in *2019 18th European Control Conference (ECC)*, pp. 2583–2588, June 2019.

[23] P. D. Labrecque and C. Gosselin, "Variable admittance for phri: From intuitive unilateral interaction to optimal bilateral force amplification," *Robotics and Computer-Integrated Manufacturing*, vol. 52, pp. 1 – 8, 2018.

[24] J. Ren, R. V. Patel, K. A. McIsaac, G. Guiraudon, and T. M. Peters, "Dynamic 3-d virtual fixtures for minimally invasive beating heart procedures," *IEEE Transactions on Medical Imaging*, vol. 27, pp. 1061–1070, Aug 2008.

[25] H. C. Lin, K. Mills, P. Kazanzides, G. D. Hager, P. Marayong, A. M. Okamura, and R. Karam, "Portability and applicability of virtual fixtures across medical and manufacturing tasks," in *Proceedings 2006 IEEE International Conference on Robotics and Automation, 2006. ICRA 2006.*, pp. 225–230, May 2006.

[26] Y. Maeda, T. Hara, and T. Arai, "Human-robot cooperative manipulation with motion estimation," in *Intelligent Robots and Systems, 2001. Proceedings. 2001 IEEE/RSJ International Conference on*, vol. 4, pp. 2240–2245, IEEE, 2001.

[27] Y. Karayiannidis, C. Smith, F. E. Vina, and D. Kragic, "Online kinematics estimation for active human-robot manipulation of jointly held objects," in *Intelligent Robots and Systems (IROS), 2013 IEEE/RSJ International Conference on*, pp. 4872–4878, IEEE, 2013.

[28] D. Papageorgiou and Z. Doulgeri, "A kinematic controller for human-robot handshaking using internal motion adaptation," in *Robotics and Automation (ICRA), 2015 IEEE International Conference on*, pp. 5622–5627, IEEE, 2015.

[29] B. Corteville, E. Aertbelien, H. Bruyninckx, J. D. Schutter, and H. V. Brussel, "Human-inspired robot assistant for fast point-to-point movements," in *Proceedings 2007 IEEE International Conference on Robotics and Automation*, pp. 3639–3644, April 2007.

[30] A. Mörtl, M. Lawitzky, A. Kucukyilmaz, M. Sezgin, C. Basdogan, and S. Hirche, "The role of roles: Physical cooperation between humans and robots," *The International Journal of Robotics Research*, vol. 31, no. 13, pp. 1656–1674, 2012.

[31] L. B. Rosenberg, "Virtual fixtures: Perceptual tools for telerobotic manipulation," in *Virtual Reality Annual International Symposium, 1993., 1993 IEEE*, pp. 76–82, IEEE, 1993.

[32] J. E. Colgate, M. Peshkin, and S. H. Klostermeyer, "Intelligent assist devices in industrial applications: a review," in *Proceedings 2003 IEEE/RSJ International Conference on Intelligent Robots and Systems (IROS 2003) (Cat. No.03CH37453)*, vol. 3, pp. 2516–2521 vol.3, Oct 2003.

[33] F. Ryden, A. Stewart, and H. J. Chizeck, "Advanced telerobotic underwater manipulation using virtual fixtures and haptic rendering," in *2013 OCEANS - San Diego*, pp. 1–8, Sept 2013.

[34] B. Siciliano and O. Khatib, eds., *Springer Handbook of Robotics*. Springer International Publishing, 2016.

[35] H. Boessenkool, D. A. Abbink, C. J. M. Heemskerk, F. C. T. van der Helm, and J. G. W. Wildenbeest, "A task-specific analysis of the benefit of haptic shared control during telemanipulation," *IEEE Transactions on Haptics*, vol. 6, pp. 2–12, First 2013.

[36] D. P. Losey, C. G. McDonald, E. Battaglia, and M. K. O'Malley, "A review of intent detection, arbitration, and communication aspects of shared control for physical human-robot interaction," *Applied Mechanics Reviews*, vol. 70, no. 1, pp. 010804–010804–19, 2018.

[37] S. A. Bowyer, B. L. Davies, and F. R. y Baena, "Active constraints/virtual fixtures: A survey," *IEEE Transactions on Robotics*, vol. 30, pp. 138–157, Feb 2014.

[38] A. Bettini, S. Lang, A. Okamura, and G. Hager, "Vision assisted control for manipulation using virtual fixtures: Experiments at macro and micro scales," in *Robotics and Automation, 2002. Proceedings. ICRA'02. IEEE International Conference on*, vol. 4, pp. 3354–3361, IEEE, 2002.

[39] A. Bettini, P. Marayong, S. Lang, A. M. Okamura, and G. D. Hager, "Vision-assisted control for manipulation using virtual fixtures," *IEEE Transactions on Robotics*, vol. 20, no. 6, pp. 953–966, 2004.

[40] R. Castillo-Cruces and J.Wahrburg, "Virtual fixtures for autonomous error compensation for human-robot cooperative tasks," *Robotica*, vol. 28, pp. 267–277, 2010.

[41] S. A. Bowyer and F. R. y Baena, "Dissipative control for physical human–robot interaction," *IEEE Transactions on Robotics*, vol. 31, no. 6, pp. 1281–1293, 2015.

[42] M. Selvaggio, G. A. Fontanelli, F. Ficuciello, L. Villani, and B. Siciliano, "Passive virtual fixtures adaptation in minimally invasive robotic surgery," *IEEE Robotics and Automation Letters*, vol. 3, pp. 3129–3136, Oct 2018.

[43] C. Bechlioulis and G. Rovithakis, "Robust adaptive control of feedback linearizable mimo nonlinear systems with prescribed performance," *IEEE Transactions on Automatic Control*, vol. 53, no. 9, pp. 2090–2099, 2008.

[44] C. P. Bechlioulis and G. A. Rovithakis, "Robust partial-state feedback prescribed performance control of cascade systems with unknown nonlinearities," *IEEE Transactions on Automatic Control*, vol. 56, pp. 2224–2230, Sep. 2011.

[45] C. P. Bechlioulis and G. A. Rovithakis, "A low-complexity global approximation-free control scheme with prescribed performance for unknown pure feedback systems," *Automatica*, vol. 50, no. 4, pp. 1217 – 1226, 2014.

[46] A. Theodorakopoulos and G. A. Rovithakis, "Low-complexity prescribed performance control of uncertain mimo feedback linearizable systems," *IEEE Transactions on Automatic Control*, vol. 61, pp. 1946–1952, July 2016.

[47] Y. Karayiannidis and Z. Doulgeri, "Model-free robot joint position regulation and tracking with prescribed performance guarantees," *Robotics and Autonomous Systems*, vol. 60, pp. 214–226, 2012.

[48] Y. Karayiannidis, D. Papageorgiou, and Z. Doulgeri, "A model-free controller for guaranteed prescribed performance tracking of both robot joint positions and velocities," *IEEE Robotics and Automation Letters*, vol. 1, pp. 267–273, Jan 2016.

[49] A. K. Kostarigka, Z. Doulgeri, and G. A. Rovithakis, "Prescribed performance tracking for flexible joint robots with unknown dynamics and variable elasticity," *Automatica*, vol. 49, pp. 1137–1147, May 2013.

[50] E. Psomopoulou, A. Theodorakopoulos, Z. Doulgeri, and G. A. Rovithakis, "Prescribed performance tracking of a variable stiffness actuated robot," *IEEE Transactions on Control Systems Technology*, vol. 23, pp. 1914–1926, Sept 2015.

[51] C. P. Bechlioulis, Z. Doulgeri, and G. A. Rovithakis, "Guaranteeing prescribed performance and contact maintenance via an approximation free robot force/position controller," *Automatica*, vol. 48, pp. 360–365, Feb. 2012.

[52] G. S. Kanakis, F. Dimeas, G. A. Rovithakis, and Z. Doulgeri, "Prescribed contact establishment of a robot with a planar surface under position and stiffness uncertainties," *Robotics and Autonomous Systems*, vol. 104, pp. 99 – 108, 2018.

[53] P. D. Triantafyllou, G. A. Rovithakis, and Z. Doulgeri, "Constrained visual servoing under uncertain dynamics," *International Journal of Control*, vol. 92, no. 9, pp. 2099–2111, 2019.

[54] A. Theodorakopoulos, G. A. Rovithakis, and Z. Doulgeri, "An impedance control modification guaranteeing compliance strictly within preselected spatial limits," in *Intelligent Robots and Systems (IROS), 2015 IEEE/RSJ International Conference on*, pp. 2210–2215, Sept 2015.

[55] S. Stavridis, D. Papageorgiou, and Z. Doulgeri, "Dynamical system based robotic motion generation with obstacle avoidance," *IEEE Robotics and Automation Letters*, vol. 2, pp. 712–718, April 2017.

[56] A. Atawnih, D. Papageorgiou, and Z. Doulgeri, "Kinematic control of redundant robots with guaranteed joint limit avoidance," *Robotics and Autonomous Systems*, pp. –, 2016.

[57] D. Papageorgiou, A. Atawnih, and Z. Doulgeri, “A passivity based control signal guaranteeing joint limit avoidance in redundant robots,” in *2016 24th Mediterranean Conference on Control and Automation (MED)*, pp. 569–574, June 2016.
[58] L. P. Ureche and A. Billard, “Constraints extraction from asymmetrical bimanual tasks and their use in coordinated behavior,” *Robotics and Autonomous Systems*, vol. 103, pp. 222 – 235, 2018.
[59] K.-W. Nam and M.-S. Kim, “Computer graphics,” ch. Hermite Interpolation of Solid Orientations Based on a Smooth Blending of Two Great Circular Arcs on SO(3), pp. 171–183, London, UK, UK: Academic Press Ltd., 1995.
[60] J. J. Kuffner, “Effective sampling and distance metrics for 3d rigid body path planning,” in *Robotics and Automation, 2004. Proceedings. ICRA ’04. 2004 IEEE International Conference on*, vol. 4, pp. 3993–3998 Vol.4, April 2004.
[61] H. Khalil, *Nonlinear Systems*. Prentice Hall, third ed., 2002.
[62] P. M. Fitts, “The information capacity of the human motor system in controlling the amplitude of movement,” *Journal of Experimental Psychology*, vol. 47, no. 6, pp. 381–391, 1954.
[63] R. Azor, I. Bar-Itzhack, J. Deutschmann, and R. Harman, “Angular-rate estimation using delayed quaternion measurements,” *Journal of Guidance, Control, and Dynamics*, vol. 24, no. 3, pp. 436–443, 2001.
[64] J. C. Chou, “Quaternion kinematic and dynamic differential equations,” *IEEE Transactions on robotics and automation*, vol. 8, no. 1, pp. 53–64, 1992.
[65] D. P. Bertsekas, “Chapter 1 - introduction,” in *Constrained Optimization and Lagrange Multiplier Methods*, pp. 1 – 94, Academic Press, 1982.

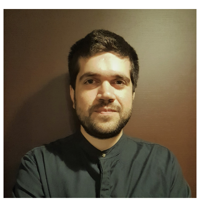

Dimitrios Papageorgiou is a postdoctoral researcher at the Automation and Robotics Lab (ARL) within the Electrical and Computer Engineering (ECE) department of the Aristotle University of Thessaloniki (AUTH), Greece. He is a graduate of ECE-AUTH and holds a PhD in control of cooperative robots from the same institution. His research interests are in the area of physical human-robot interaction and dynamical system based motion generation. He is an IEEE member (RAS and CS) and a member of the Technical Chamber of Greece.

Theodora Kastritsi was born in 1992. She is currently a Ph.D. student in the Department of Electrical and Computer Engineering, of the Aristotle University of Thessaloniki (AUTH), Greece, from where she received a diploma in Electrical and Computer Engineering in 2016. Her research interests are in the area of physical human-robot interaction and robotic-assisted surgery. She is an IEEE student member.

Zoe Doulgeri (M’90-SM’17) is a professor with the Electrical and Computer Engineering (ECE) department of the Aristotle University of Thessaloniki (AUTH), Greece. She is a graduate of ECE-AUTH, with Masters (MSc) in Control Systems and Social and Economic Studies and a PhD in production scheduling of flexible manufacturing systems from the Imperial College, London UK. Her research interests include physical human-robot interaction, object grasping and manipulation, redundant and flexible joint manipulators, and model free control of robotic systems with prescribed performance guarantees. She is an IEEE senior member (RAS and CS), the representative of Greece in the European Control Association (EUCA) and a member of the Technical Chamber of Greece.

George A. Rovithakis (S’89-M’98-SM’02) received the diploma in Electrical Engineering from the Aristotle University of Thessaloniki, Greece in 1990 and the M.S. and Ph.D degrees in Electronic and Computer Engineering both from the Technical University of Crete, Greece in 1994 and 1995 respectively. After holding a visiting Assistant Professor position with the Department of Electronic and Computer Engineering, Technical University of Crete from 1995 to 2002, he joined the Aristotle University of Thessaloniki where he is currently a Professor and the director of the Automation and Robotics Laboratory (ARL) of the Department of Electrical and Computer Engineering. His research interests include nonlinear control, robust adaptive control, prescribed performance control, robot control and control-identification of uncertain systems using neural networks, where he has authored or co-authored 3 books and over 155 papers in scientific journals, conference proceedings and book chapters. Dr. Rovithakis is currently an Associate Editor of the IEEE Transactions on Control Systems Technology and a member of the Technical Chamber of Greece. He has served for a series of years as an Associate Editor of the IEEE Transactions on Neural Networks, as a member of the IEEE Control Systems Society Conference Editorial Board and as a member of the EUCA-Conference Editorial Board.